JOURNAL OF GEOPHYSICAL RESEARCH, VOL. 104, NO. D19, PAGES 23,911–23,934, OCTOBER 20, 1999

Simulation of stratospheric tracers using an improved empirically based two-dimensional model transport formulation

Eric L. Fleming,[1] Charles H. Jackman, Richard S. Stolarski, and David B. Considine[2]
NASA Goddard Space Flight Center, Greenbelt, Maryland

Abstract. We have developed a new empirically based transport formulation for use in our Goddard Space Flight Center (GSFC) two-dimensional chemistry and transport model. In this formulation, we consider much of the information about atmospheric transport processes available from existing data sets. This includes zonal mean temperature, zonal wind, net heating rates, and Eliassen-Palm flux diagnostics for planetary and synoptic-scale waves. We also account for the effects of gravity waves and equatorial Kelvin waves by utilizing previously developed parameterizations in which the zonal mean flow is constrained to observations. This scheme utilizes significantly more information compared to our previous formulation and results in simulations that are in substantially better agreement with observations. The new model transport captures much of the qualitative structure and seasonal variability observed in stratospheric long lived tracers, such as isolation of the tropics and the southern hemisphere winter polar vortex, the well-mixed surf-zone region of the winter subtropics and midlatitudes, and the latitudinal and seasonal variations of total ozone. Model simulations of carbon 14 and strontium 90 are in good agreement with observations, capturing the peak in mixing ratio at 20-25 km and the decrease with altitude in mixing ratio above 25 km. We also find mostly good agreement between modeled and observed age of air determined from SF_6 outside of the northern hemisphere polar vortex. However, inside the vortex, the model simulates significantly younger air compared to observations. This is consistent with the model deficiencies in simulating CH_4 in this region and illustrates the limitations of the current climatological zonal mean model formulation. The model correctly propagates the phase of the lower stratospheric seasonal cycles in $2CH_4+H_2O$ and CO_2. The model also qualitatively captures the observed decrease in the amplitude of the stratospheric CO_2 seasonal cycle between the tropics and midlatitudes. However, the simulated seasonal amplitudes were attenuated too rapidly with altitude in the tropics. The generally good model-measurement agreement of these tracer simulations demonstrate that a successful formulation of zonal mean transport processes can be constructed from currently available atmospheric data sets.

1. Introduction

Two-dimensional (2-D) chemistry and transport models have been used extensively to study various natural physical processes in the middle atmosphere and to assess the long-term impact of human activity on stratospheric ozone. Recent emphasis has been put on model studies and assessments of long-term ozone changes due to perturbations in the lower and middle stratosphere. Such perturbations include anthropogenic chlorine loading [*World Meterological Organization (WMO)*, 1995], the injection and dispersion of volcanic aerosols [e.g., *Solomon et al.*, 1996; *Jackman et al.*, 1996; *Rosenfield et al.*, 1997], and the projected emissions of supersonic aircraft [e.g., *Stolarski et al.*, 1995]. In the lower and middle stratosphere, ozone has a relatively long photochemical lifetime and is strongly influenced by the dynamics in this region. Therefore for 2-D models, proper representation of zonal mean transport processes below

[1] Also at Steven Myers and Associates Corporation, Arlington, Virginia.

[2] Also at Department of Meteorology, University of Maryland, College Park.

Paper number 1999JD900332.
0148-0227/99/1999JD900332$09.00

$\sim$ 35 km is crucial in providing reasonable model simulations of stratospheric ozone.

We have recently developed an upgraded empirical transport formulation that utilizes several quantities derived from observational data sets: zonal mean temperature, zonal wind, net heating rates, and Eliassen-Palm flux diagnostics for planetary- and synoptic-scale waves. We also use the parameterizations of *Lindzen* [1981] and *Holton and Zhu* [1984] to account for the effects of gravity waves in which the zonal mean flow is constrained to observations. In a similar fashion, we use the parameterization of *Dunkerton* [1979] to account for the effects of equatorial Kelvin waves. These quantities are then used to derive self-consistent residual circulation and diffusion fields. The unique approach here is that we have incorporated these wave parameterizations and explicit diagnostic quantities into one comprehensive, empirically based transport scheme. Such a scheme should be able to resolve more of the details of middle atmospheric transport compared to our previous empirically based formulations.

Historically, it has been difficult to validate model dynamical fields given the sparsity of available observations and the competing roles of transport and photochemistry on model simulations of ozone and long-lived tracers. Previously, observations of radioactive debris from nuclear bomb tests during the 1960s provided a means of validating model transport in the upper troposphere and lower stratosphere [*Prather and Remsberg*, 1993; *Kinnison et al.*, 1994]. However, these model-measurement comparisons were limited by the sparse observations available. More recently, high-quality measurements of SF_6 [*Elkins et al.*, 1996; *Harnisch et al.*, 1996; *Ray et al.*, 1999] and CO_2 [*Boering et al.*, 1996] from several aircraft and balloon in-situ campaigns, and long term satellite measurements of H_2O and CH_4 from the Upper Atmosphere Research Satellite (UARS) [*Mote et al.*, 1998; *Randel et al.*, 1998], provide a powerful database from which stratospheric transport rates can be characterized. These observations therefore provide a means to more fully evaluate model transport through various model-measurement comparisons.

The purpose of this paper is to provide a detailed evaluation of our new 2-D model transport formulation in the upper troposphere and stratosphere. We have performed several diagnostic tests of the model transport and will show model-data comparisons of total ozone, CH_4, the inert radioactive tracers carbon 14 and strontium 90, age of air derived from SF_6, and the propagation of seasonal cycles in CO_2 and the quantity $2CH_4 + H_2O$. Through these extensive model-measurement comparisons, we demonstrate that our new empirically based transport scheme can successfully reproduce many of the transport-sensitive features observed in the stratosphere.

2. GSFC 2-D Model

The 2-D model at NASA Goddard Space Flight Center (GSFC) was originally described by *Douglass et al.* [1989] and extended to mesospheric heights by *Jackman et al.* [1990]. The model has recently undergone significant development in several areas, including improvements in the method of computing the photolytic source term and the photolysis of O_2 [*Jackman et al.*, 1996]. We have also recently updated the model reaction rates and photolysis cross sections to the Jet Propulsion Laboratory (JPL) 1997 recommendations [*DeMore et al.*, 1997].

As discussed by *Jackman et al.* [1996], we have made significant improvements to the model transport formulation. In this paper, we validate this new scheme by presenting detailed model-measurement comparisons of long-lived tracers in the lower and middle stratosphere. We note that the transport has undergone some minor changes since the recent Models and Measurements II (MMII) intercomparison project, so that the results shown here will differ somewhat from those presented in the MMII publications [*Hall et al.*, 1999; *Park et al.*, 1999]. This new scheme is summarized below.

The methodology generally follows that of interactive 2-D models [e.g., *Garcia et al.*, 1992; *Bacmeister et al.*, 1995], as originally formulated by *Garcia and Solomon* [1983]. However, the new transport fields are based on empirical data sets as opposed to being computed interactively in the model. A meridional stream function ($\bar{\chi}^*$) is calculated to obtain the transformed Eulerian circulation ($\bar{v}^*, \bar{w}^*$). The coefficients of the elliptic stream function equation depend on the zonal mean temperature and zonal wind, which are based on the 17 year average (1979-1995) of temperature data from the National Centers for Environmental Prediction (NCEP) for 1000-1 mbar, and the CIRA-86 empirical reference model for the mesosphere above 1 mbar [*Fleming et al.*, 1990]. Outside of the tropics, the zonal mean winds are derived from temperature using the gradient wind relation, with wind measurements from the high resolution Doppler imager (HRDI) on board UARS used for the zonal winds at tropical latitudes (20°S-20°N). We have merged the zonal mean temperature and wind data sets in a manner that maintains exact thermal wind balance throughout the model domain, as necessitated by the stream function formulation.

Forcing of the stream function is proportional to: (1) the vertical gradient of the mechanical forcing from planetary- and synoptic-scale waves, gravity waves, and equatorial Kelvin waves; and (2) the latitudinal gradient of the total heating rate which is comprised of diabatic, latent, and net eddy heating from gravity waves and planetary- and synoptic-scale waves.

Planetary wave forcing is proportional to the Eliassen-Palm (E-P) flux divergence [e.g., *Andrews et al.*, 1987]

which we have computed offline from the 17-year NCEP 3-D analyses for 1000-1 mbar and the CIRA-86 planetary wave climatology [*Barnett and Labitzke*, 1990] for the mesosphere above 1 mbar. Eddy winds are derived from the balanced wind relation poleward of ±20°, with HRDI measurements used for 20°S-20°N. Following *Randel and Garcia* [1994], latitudinal eddy diffusion (K_{yy}) is obtained self-consistently as the ratio of the E-P flux divergence to the latitudinal gradient of zonal mean potential vorticity ($\bar{q}_y$). To approximate the circulation associated with the equatorial semiannual oscillation (SAO), we use the methodology of *Dunkerton* [1979] and *Gray and Pyle* [1987] along with the empirical zonal mean wind field to diagnose the mechanical forcing from thermally damped equatorial Kelvin waves.

To obtain distributions of vertical eddy diffusion (K_{zz}) and mechanical forcing from gravity waves in the mesosphere and upper stratosphere, we use the parameterization originally developed by *Lindzen* [1981] and modified by *Holton and Zhu* [1984]. Here, we utilize the empirical zonal mean temperature and zonal wind fields (described above) in the parameterization to diagnose the latitudinal, seasonal, and vertical distributions of gravity wave drag and diffusion based on a given set of gravity wave parameters. In the troposphere and lower stratosphere, we scale K_{zz} based on the vertical temperature gradient, so that a stronger lapse rate, indicative of more rapid convective overturning, implies a larger value of diffusion. This methodology gives a large mixing rate in the troposphere and a very small K_{zz} in the lower stratosphere, with a sharp gradient across the tropopause boundary. We specify a lower limit on K_{zz} of 0.01-0.02 m^2s^{-1} in the lower stratosphere following the observational analyses of *Hall and Waugh* [1997b] and *Mote et al.* [1998].

Diabatic heating rates are computed following *Rosenfield et al.* [1994], utilizing climatological distributions of temperature, ozone, and water vapor. The climatological latent heating rate distribution is adapted from *Newell et al.* [1974]. Net gravity wave heating is computed following *Schoeberl et al.* [1983] and *Huang and Smith* [1991], utilizing the vertical diffusion rates computed from the gravity wave parameterization discussed above. Eddy heating from planetary- and synoptic-scale waves [e.g., *Andrews et al.*, 1987] is computed from the 3-D meteorological fields discussed above.

To obtain a reasonable circulation in the troposphere and lower stratosphere, it is necessary to impose a suitable lower tropospheric boundary condition on the stream function at 760 mbar. Following *Garcia et al.* [1992], this is computed from the integral of the total zonal momentum forcing above the 760 mbar surface at each latitude. This follows from the downward control principle under quasi-geostrophic scaling [e.g., *Haynes et al.*, 1991] and generally results in upward motion out of the boundary layer equatorward of ±50° and downward motion into the boundary layer at higher latitudes.

We have implemented a new numerical advection algorithm replacing the previous scheme based on *Prather* [1986]. The new algorithm is a 2-D version of the flux form scheme developed by *Lin and Rood* [1996] currently used in the GSFC 3-D chemistry and transport model [*Douglass et al.*, 1996]. The new scheme is mass conserving and utilizes an upstream piecewise parabolic method (PPM) [*Colella and Woodward*, 1984; *Carpenter et al.*, 1990]. We use the fully monotonic PPM so that no new minima or maxima are generated by advection. This algorithm includes cross terms to account for errors produced by operator splitting, i.e., the successive application of meridional and vertical advection operators. A time step of 12 hours is used for the advection of constituents. The PPM is highly accurate (to fourth order) and preserves sharp tracer gradients quite well, while exhibiting very little numerical diffusion. This was found to be especially important for simulations in regions of strong wind shear and sharp gradients in the tracer field, such as water vapor near the tropical tropopause.

3. Results

We now compare the spatial structure and seasonal evolution of model-simulated tracer fields with observations. We first show CH_4 and ozone from our standard model which has been run for 20 years to obtain a seasonally repeating steady state solution. We then show results from time dependent simulations of SF_6, CO_2, and radioactive products of atmospheric nuclear bomb tests, carbon 14 and strontium 90, to illustrate more detailed aspects of the model transport in the upper troposphere and stratosphere. We also compare our new model simulations with those using the previous version of the model transport to illustrate how the new methodology improves the tracer simulations.

3.1. Methane

Figure 1 shows latitude-height sections of methane from the model simulation (solid contours) and observations (dashed contours) for the months indicated. Here we compare with the combined climatology compiled by *Randel et al.* [1998] based on data from the Halogen Occultation Experiment (HALOE) and the Cryogenic Limb Array Etalon Spectrometer (CLAES) instruments aboard UARS. The CLAES data have been used to fill in the high-latitude regions during winter where HALOE does not obtain measurements. This climatology has been averaged using potential vorticity (PV) as a horizontal coordinate and then mapped to equivalent latitude (the latitude of an equivalent PV

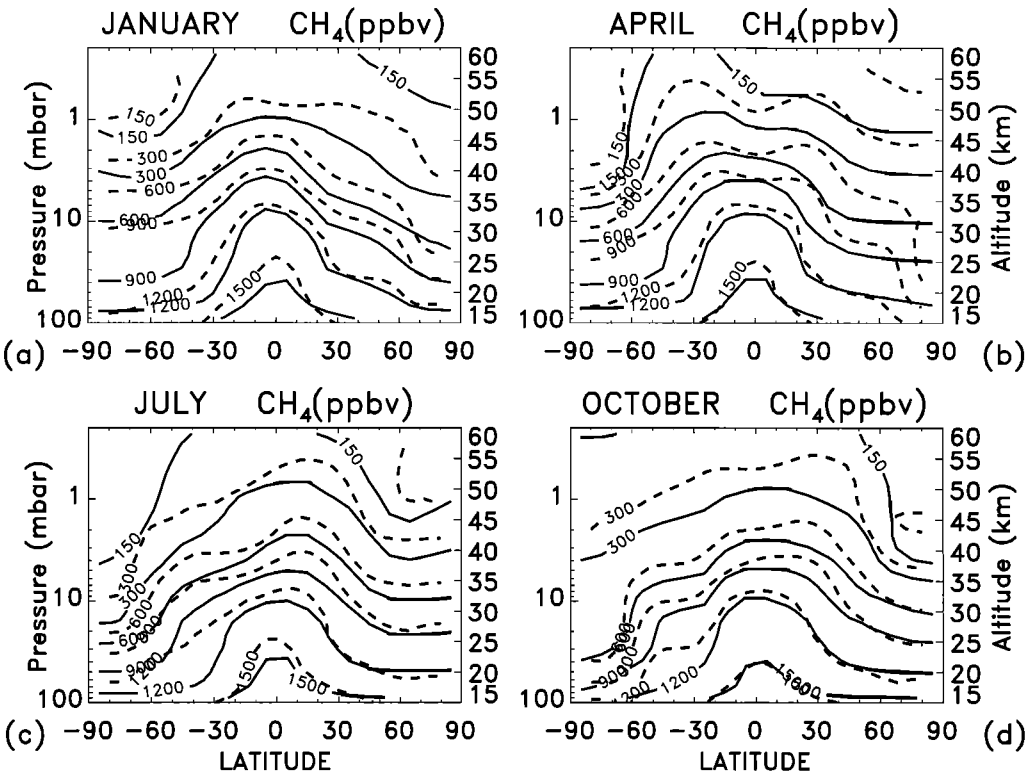

Figure 1. Zonal mean CH_4 (ppbv) from the model simulation (solid line) and the HALOE+CLAES climatology (dashed line) for January, April, July, and October. The contour interval is 300 ppbv, and the 150 ppbv contour is included.

distribution arranged symmetrically about the pole; see *Randel et al.* [1998] for details). This averaging procedure increases the effective latitudinal coverage of the data. Results are similar to standard latitude averaging except at high northern latitudes during winter and spring, when the vortex can be significantly displaced from the pole.

The structure and seasonal variations of the model compare qualitatively well with the data. Characteristic dynamical features are evident, such as the steep horizontal gradients in the subtropics associated with the isolation of the tropics, and the weak gradients of the well-mixed surf-zone region of the winter midlatitudes. The model captures the isolation of the southern hemisphere (SH) vortex in October in the lower and middle stratosphere. In the upper stratosphere, flat tracer gradients indicating strong horizontal mixing into the polar region are evident during October in both the data and model (the 300 ppbv contour). Note also the high-latitude descent during autumn in the upper stratosphere is evident in both hemispheres. Small CH_4 values characteristic of mesospheric air extend down to 35-40 km in both the model and data.

The comparison in Figure 1 also shows some model discrepancies. For example, the absolute values of CH_4 in the model tend to be underestimated in the middle and upper stratosphere. Also, the model does not fully resolve the isolation of the northern polar vortex observed in January. This is not surprising since this region experiences large longitudinal variability which is accounted for in the equivalent latitude mapping of the data, but is not resolved with the standard zonal mean model formulation. In contrast, the southern polar region during winter and early spring typically exhibits less variability, so that the model agrees fairly well with the data in this region in Figure 1.

The UARS climatology for April shows the well-known "double-peaked" structure at low latitudes in the upper stratosphere. This feature is associated with the meridional circulation induced by the SAO and is most pronounced during the NH spring. The model shows some indication of this feature above 45 km but underestimates the overall magnitude and does not reveal the SAO signature below ~45 km seen in the observations. Similar findings were reported in other modeling studies of the SAO which used climatological data sets to derive the zonal mean transport fields [*Choi and Holton*, 1991], and results from the NCAR MACCM2 3-D model simulations [*Randel et al.*, 1994; *Waugh et al.*, 1997].

3.2. Ozone

Our model total ozone simulation and comparison with the Total Ozone Mapping Spectrometer (TOMS) version 7 data were reported by *Jackman et al.* [1996].

Since that publication, the simulation has improved somewhat in the SH midlatitudes, and we provide a summary of our current model-TOMS comparison here. Figure 2 shows the model total ozone for 1990 conditions of total chlorine loading, along with the TOMS data averaged over 1988 to 1992, and the difference (model minus TOMS). Much of the observed seasonal structure is qualitatively simulated by the model, including the on-the-pole maximum of ~440 Dobson units (DU) during the NH spring and the minimum in the NH autumn; the seasonality in the tropics, with a maximum during October, a secondary maximum during April, and a minimum during the NH winter; the off-the-pole maximum during the southern late winter-spring; and the very low ozone at the southern pole characterizing the Antarctic ozone hole during spring.

There are some notable discrepancies in the simulation: (1) the model overpredicts total ozone at NH midlatitudes during summer and early fall; (2) the magnitude of the simulated southern off-the-pole-maximum is not as large as observed; and (3) the model does not simulate the near elimination of strong latitudinal gradients at high southern latitudes observed following the breakup of the ozone hole. The model also shows noticeably less ozone compared to TOMS at high southern latitudes during summer and early fall. To check if discrepancy 3 is due to an underestimation of horizontal mixing during the spring breakup of the Antartic vortex, we performed an additional model run with K_{yy} set to a very large value of $4\text{x}10^{10}\text{cm}^2\text{s}^{-1}$ poleward of 50°S throughout the lower stratosphere during October and November. However, this gave only a marginal improvement compared to the standard model simulation. This suggests that other deficiencies in the model are causing the larger than observed latitudinal gradients during the austral spring and summer. We note that the model dynamical fields have been contructed from a 17-year average (1979-1995) of NCEP data, whereas the TOMS observations in Figure 2 are taken as a 5-year average for 1988-1992. This difference may account for some of these model-measurement discrepancies.

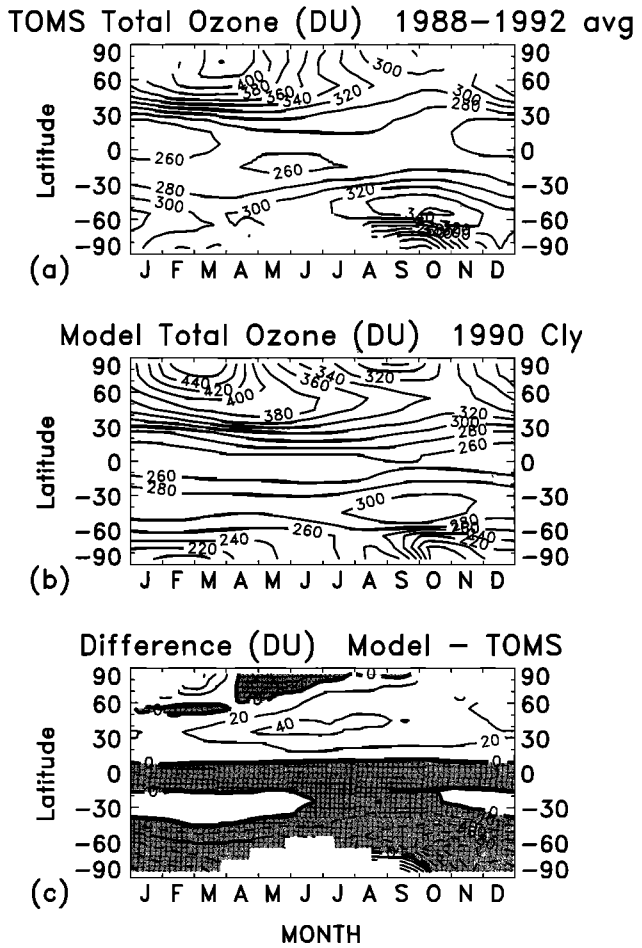

Figure 2. Zonal and monthly mean total ozone from (a) Nimbus 7 TOMS version 7 data averaged over 1988 to 1992, (b) the model simulation corresponding to 1990 Cl_y loading, and (c) the difference, model minus TOMS. The contour interval is 20 Dobson units (DU).

Our model profile ozone simulations were previously compared with NOAA 11 Solar Backscattered Ultraviolet 2 (SBUV/2) data as discussed by *Jackman et al.* [1996]. In Figure 3 we compare model vertical ozone profiles for several latitudes and seasons with the 1988-1996 climatology based on the Stratospheric Aerosol and Gas Experiment (SAGE) II and ozone sonde data. This was compiled by J. Logan and R. McPeters for the MMII intercomparison project [*Park et al.*, 1999]. In the lower stratosphere below ~30 km, the model shows good agreement with the data in most of the comparisons. An exception is at 75°S during January, where the model underestimates the data between the tropopause and 25 km. This results in the model underestimating the total column ozone relative to TOMS in the SH high-latitude summer as seen in Figure 2. At 45°N during July (Figure 3b), the model shows a small overestimation of the observed ozone at all levels between the tropopause and 30 km. This is reflected in the overprediction of the model total column ozone relative to TOMS in the NH midlatitude summer in Figure 2. In the region above 35 km, the model shows a systematic underestimation of the observed ozone at most latitudes and seasons. This well-known "ozone deficit" problem in our model is caused by an overprediction of chlorine radicals. This problem can be significantly reduced when including the reaction $\text{ClO} + \text{OH} - > \text{HCl} + \text{O}_2$ in the model chemistry [e.g., *Chandra et al.*, 1993; *Lipson et al.*, 1997]. However, this reaction is not included in our present model, which follows the current JPL-1997 recommendations [*DeMore et al.*, 1997].

3.3. Carbon 14 and Strontium 90

The radioactive products of atmospheric nuclear bomb tests, carbon 14 (^{14}C) and strontium 90 (^{90}Sr), are very useful in testing the transport in a model [e.g., *Jackman et al.*, 1991; *Prather and Remsberg*, 1993; *Kinnison et al.*, 1994]. These compounds have chemical lifetimes

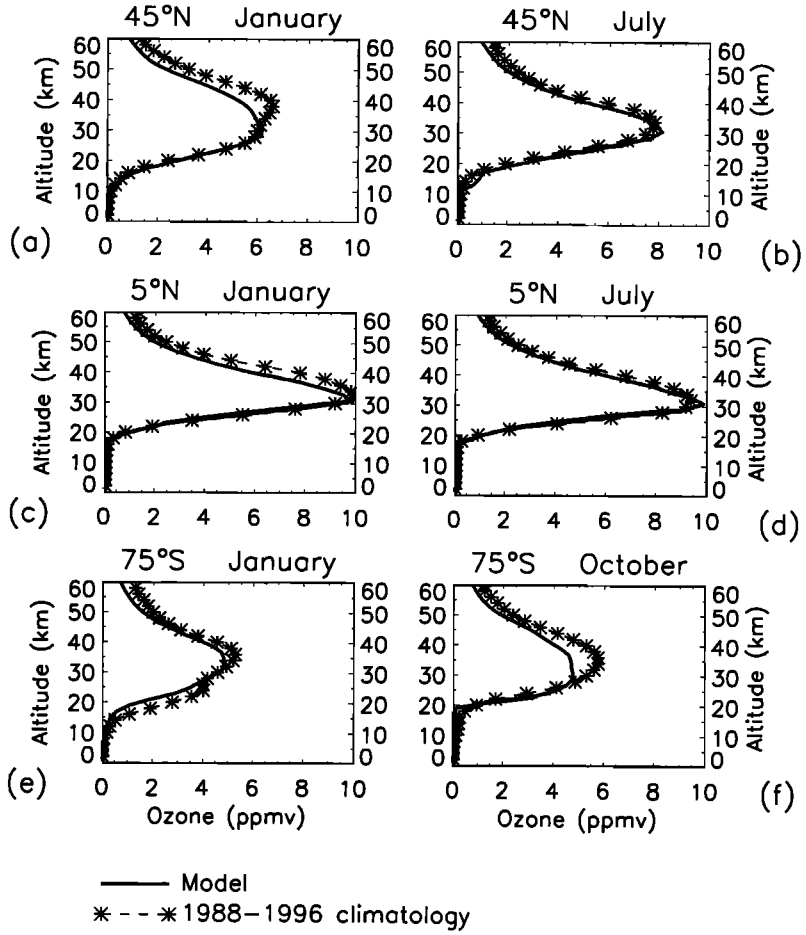

Figure 3. Vertical profiles of ozone mixing ratio (ppmv) for the latitudes and months indicated. Shown are the model simulation (solid line) and the 1988-1996 climatology (dashed line-asterisk) compiled by J. Logan and R. McPeters [see *Park et al.*, 1999]. The climatology is based on a combination of SAGE II and ozonesonde data.

and lower stratospheric source regions which are similar to long-lived products of supersonic aircraft exhaust. Therefore model-measurement comparisons of ^{14}C and ^{90}Sr are especially helpful in evaluating the accuracy of model assessments of the effects of stratospheric aircraft.

The initial conditions for ^{14}C and ^{90}Sr input into our model were taken from *Prather and Remsberg* [1993], and their latitude and altitude dependent distributions were specified on October 15, 1963, and on October 15, 1964, respectively. Time and hemisphere dependent ground boundary conditions for ^{14}C and latitude and altitude dependent settling velocities for ^{90}Sr were also specified from *Prather and Remsberg* [1993].

Our time dependent simulation of ^{14}C is shown in Figure 4 for the months of January and July in 1964, 1965, and 1966. The peak at middle to high latitudes persists through July 1965, although the model transport moves the enhanced ^{14}C in the tropical lower stratosphere up through the middle (January 1965) and upper (July 1965) stratosphere before being totally dissipated (January 1966). Strong gradients in the northern lower stratosphere between the tropics and extratropics persist through January 1966, indicating the very slow transport and mixing that takes place in this region. The final distribution shown in July 1966 is similar to that of a long-lived source gas (see CH_4 in Figure 1), except the largest amounts of ^{14}C are found in the upper stratosphere with smaller amounts at lower altitudes. It thus takes about 3 years for a primarily NH lower stratospheric source distribution of a substance to become relatively well mixed throughout the stratosphere.

Detailed comparisons between the model and measurements at 31°N are shown in Figure 5. Also shown are model results from an older version (designated the 1995 model) as well as the new version of our model transport (designated the 1999 model). The 1999 model is clearly an improvement over the 1995 model during the period of the ^{14}C simulation. The ^{14}C peak between 20 and 25 km and the very large gradient between 10 and 20 km in the measurements are represented much better by the 1999 model.

We also show comparisons of ^{90}Sr between the two

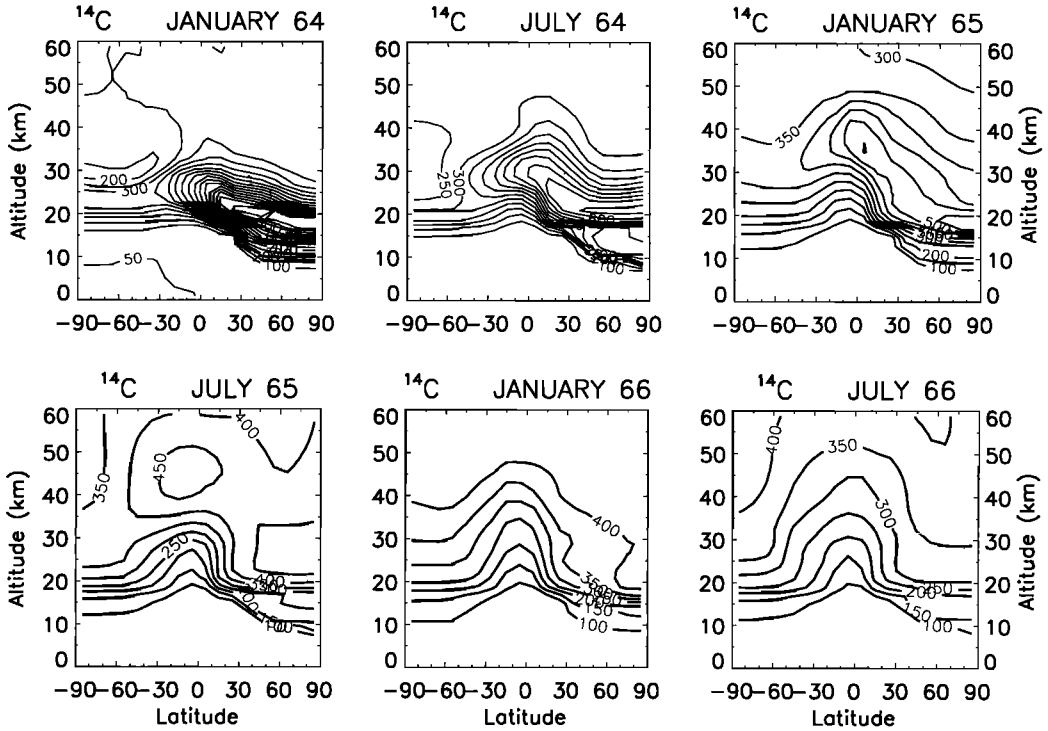

Figure 4. Time dependent model simulations of carbon 14 (^{14}C) every 6 months between January 1964 and July 1966. The contour interval is 50 mixing ratio units, defined as 10^5 atoms of ^{14}C per gram of dry air [*Kinnison et al.*, 1994].

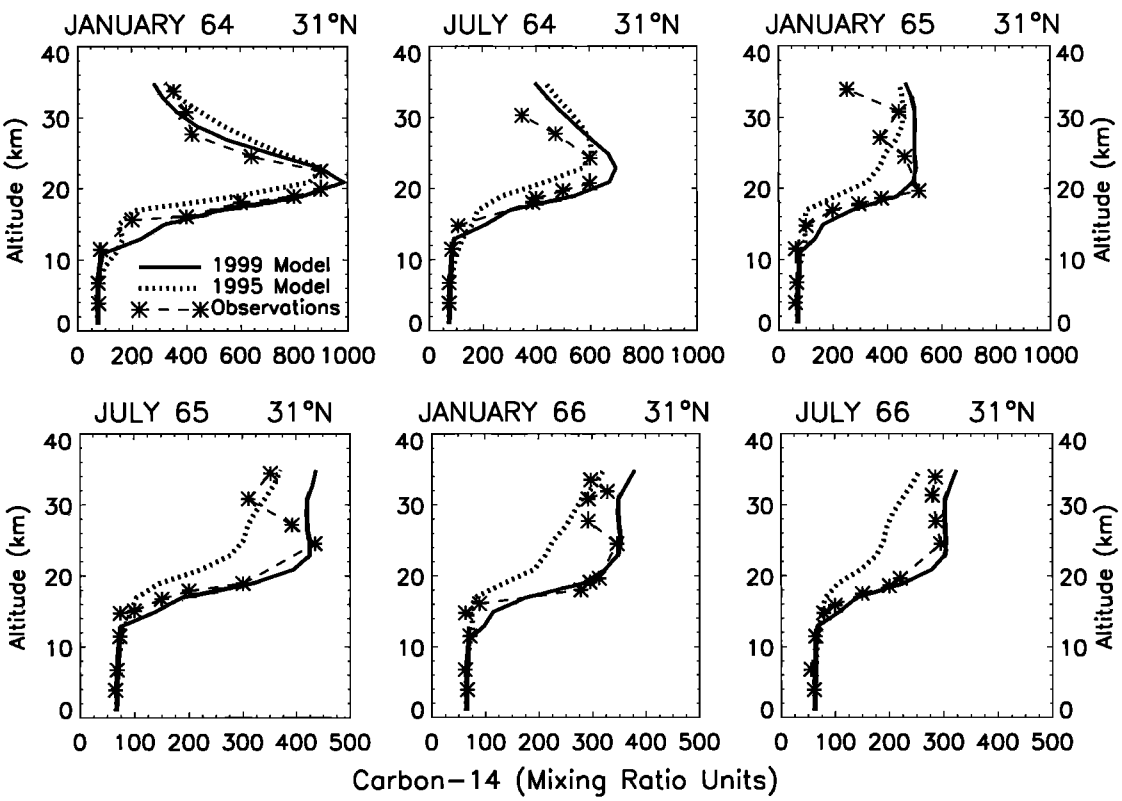

Figure 5. Vertical profiles of carbon 14 at 31°N every 6 months between January 1964 and July 1966. Plotted are the time dependent model simulations using the new transport formulation (solid), the previous 1995 transport formulation (dotted), and observations (*Kinnison et al.* [1994], dashed-asterisk). Values are in mixing ratio units, defined as 10^5 atoms of ^{14}C per gram of dry air.

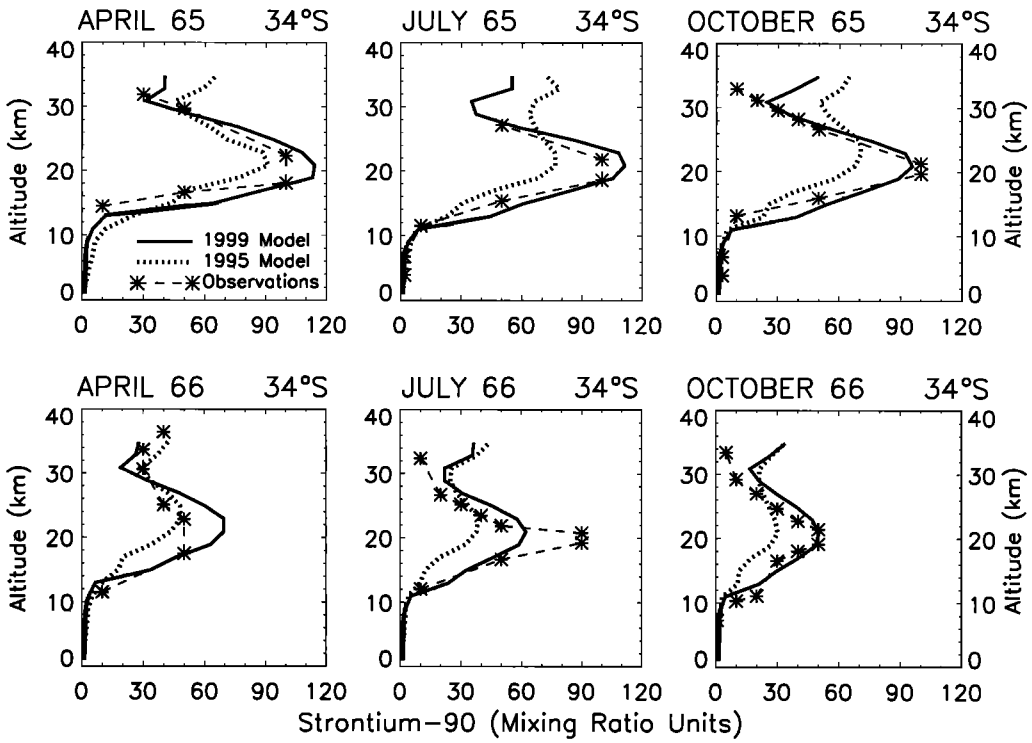

Figure 6. Vertical profiles of strontium 90 at 34°S for six time periods between April 1965 and October 1966. Plotted are the time dependent model simulations using the new transport formulation (solid), the previous 1995 transport formulation (dotted), and observations (*Kinnison et al.* [1994], dashed-asterisk). Units are proportional to mixing ratio as in the work by *Kinnison et al.* [1994]. Model simulations include a settling velocity for strontium 90 as discussed in the text.

versions of our model and the measurements at 34°S in Figure 6. Again it is apparent that the 1999 model simulates ^{90}Sr more realistically than the 1995 model. Similar comparisons between the two model versions were also seen at tropical latitudes (9°N, not shown). The two model simulations in Figure 6 especially diverge from one another in late 1965. The excellent agreement between the 1999 model and the measurements in October 1966 may be fortuitous, given that the real atmosphere undergoes interannual dynamical variability that is not contained in our 1999 model transport. It is significant, however, that the modeled ^{90}Sr generally simulates the gradual decrease of measured stratospheric ^{90}Sr over 1965 and 1966, while representing the peak concentration at 20-25 km in a very reasonable manner.

There are substantial differences between our 1999 model and 1995 model transport formulations which are reflected in these ^{14}C and ^{90}Sr simulations. While the advective transport by the mean circulation exhibits some differences, much of the changes seen in Figures 4-6 are due to changes in the meridional and vertical diffusive transport. The 1999 model is generally less diffusive in a globally averaged sense. However, more important, the sharp changes in diffusion that occur across certain atmospheric regions are much better resolved in the 1999 model. These include the changes in vertical mixing across the tropopause, and the changes in horizontal mixing between the tropics, subtropics, and midlatitudes in the stratosphere.

3.4. Age of Air From SF_6

Sulfur hexafluoride (SF_6) is a nearly inert anthropogenically produced tracer. It has had a relatively steady source at the ground over the past 2-3 decades, allowing for a quasi-linear temporal increase in atmospheric concentration [e.g., *Geller et al.*, 1997]. The time lag of SF_6 between a given point in the stratosphere and a reference location at the ground determines the mean age of air, Γ [*Elkins et al.*, 1996; *Harnisch et al.*, 1996]. This has become a widely used diagnostic of model transport [e.g., *Hall and Plumb*, 1994; *Waugh et al.*, 1997; *Hall et al.*, 1999]. The annually averaged Γ derived from stratospheric SF_6 above the 380 K potential temperature surface is very similar to the mean age determined from the first moment of the age spectrum in model simulations [*Hall and Plumb*, 1994; *Hall and Waugh*, 1997a; *Hall et al.*, 1999]. In addition, seasonal variations of the stratospheric age determined from SF_6 can be significant.

Our model simulations of Γ determined from SF_6 for January and October are shown in Figure 7. Here we

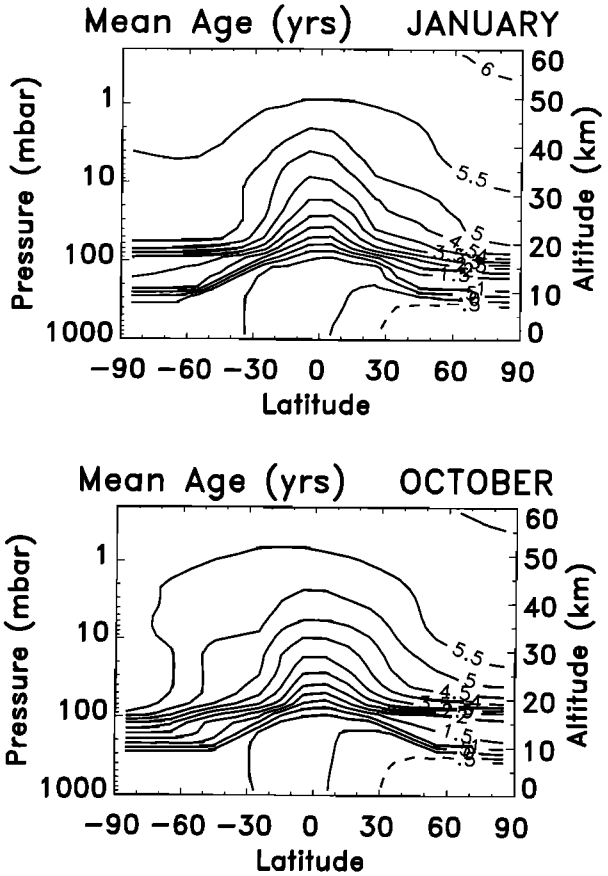

Figure 7. Mean age of air (years) derived from time dependent model simulations of SF_6 for January and October. The age is taken relative to the global mean value at the surface. The contour interval is 0.5 years.

have taken the area weighted global mean value at the surface as the reference point and have accounted for the small nonlinear effect in the time increase of SF_6 [*Volk et al.*, 1997]. This nonlinear effect slightly increases the mean age compared to the simple time lag method, with the difference approaching 0.5 years for Γ of ~6 years. In the troposphere, the interhemispheric gradient of SF_6 makes the one-to-one relationship between mean age and the mean value of SF_6 ambiguous. We note however, that there is a 1-1.5 year time lag between midlatitudes of the NH and SH in the troposphere. This interhemispheric exchange time is in good agreement with SF_6 measurements [e.g., *Harnisch et al.*, 1996; *Geller et al.*, 1997].

The very lower stratosphere exhibits sharp vertical gradients in age due to the drastic reduction in vertical mixing across the tropopause into the lower stratosphere. The age of air contour shapes in the stratosphere are qualitatively similar to other long-lived tracers (e.g., CH_4, Figure 1), consistent with the mean circulation. The youngest stratospheric air occurs just above the tropical tropopause (about 4 months older than the global mean surface value), with the oldest air of 6-6.5 years occurring in the mesosphere and polar winter upper stratosphere. The mean age in the mesosphere is relatively uniform owing to the vigorous meridional circulation and vertical mixing characteristic of this region. The older ages seen in the polar stratosphere in fall and winter are indicative of the descent of older mesospheric air within the polar vortex. As expected, this feature is more pronounced in the SH where, relative to the NH, the polar vortex is more isolated from the younger midlatitude air. The isolation of the SH polar region in the lower stratosphere persists into October, as indicated by the local maximum in Γ centered near 50 mbar at the South Pole in Figure 7. This isolation was also reflected in the CH_4 simulation in Figure 1.

Observations of Γ can be made in certain regions using measurements of SF_6 from aircraft [*Elkins et al.*, 1996], balloons [*Harnisch et al.*, 1996; *Patra et al.*, 1997; F.L. Moore et al., manuscript in preparation, 1999], and the space shuttle [*Rinsland et al.*, 1993]. Mean ages can also be derived from CO_2 measurements after taking into account the annual cycle in CO_2 at the ground and a small correction for CH_4 oxidation [e.g., *Boering et al.*, 1996; *Andrews et al.*, 1999]. Ages derived from CO_2 in this way were found to be similar to those derived from SF_6 data at 20 km [*Waugh et al.*, 1997; *Hall et al.*, 1999].

Figure 8 shows the mean age for October/November 1994 computed from the model at 20 km compared with that derived from SF_6 data at 19-21 km taken from the Airborne Chromatograph for Atmospheric Trace Species (ACATS) instrument onboard several NASA ER-2 flights [*Elkins et al.*, 1996]. The global mean surface time series of *Geller et al.* [1997] is used as the reference point for the SF_6 measurements. Again for both the model and observations, we have accounted for the small nonlinear effect in the time increase of SF_6 [*Volk et al.*, 1997]. The base 1999 model simulation (solid line) in Figure 8 captures much of the latitudinal variation seen in the data, including the sharp gradient between the equator and ±20°. Ages near the equator are ~1.5 years in both the model and data. While there is a fairly large spread in the observations at middle and higher latitudes, the model Γ tends to be close to the average of the data points in these regions.

Figure 9 shows vertical profiles of Γ from the model and balloon SF_6 data of *Harnisch et al.* [1996] (asterisks and squares) and the Observations of the Middle Stratosphere (OMS) campaign Lightweight Airborne Chromatography Experiment (LACE) instrument (F.L. Moore et al., manuscript in preparation, 1999) (triangles), for the latitudes and seasons indicated. Again we have used the global mean value at the surface as the reference function [*Geller et al.*, 1997] which gives stratospheric ages that are 0.25 to 1 year younger than those derived using the NH tropospheric reference function of *Harnisch et al.* [1996]. At all latitudes in Figure 9, the vertical gradient of Γ from the the standard 1999 model (solid line) agrees rather well with the data in

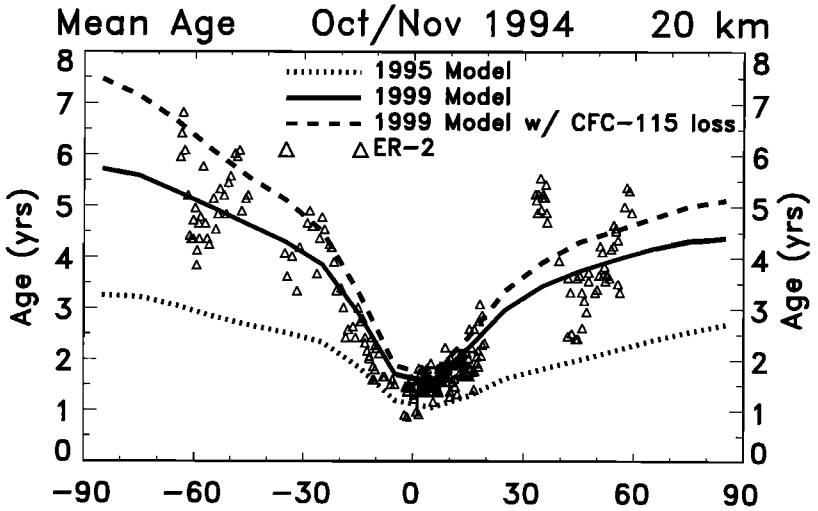

Figure 8. Age of air derived from SF_6 as a function of latitude for October/November 1994 using ER-2 measurements at 19-21 km (triangles) and model simulations at 20 km (lines). Included are model simulations using the previous 1995 model transport (dotted line), the 1999 transport (solid line), and the 1999 transport with a photochemical loss identical to CFC-115 imposed on SF_6 (dashed line). The age is taken relative to the global mean value at the surface.

the very lower stratosphere below ~20-22 km. This includes the transition from very weak gradients in the troposphere to much stronger gradients in the lower stratosphere. This is consistent with the model-data comparisons of ^{14}C and ^{90}Sr seen in Figures 5 and 6. Above ~25 km, the data generally indicate a transition to little or no vertical gradient, and the 1999 model qualitatively reproduces this feature in most of the comparisons.

In Figure 9, the model above ~22 km agrees well with the data at 44°N but not as well at 35°N. These data show age differences of about 1 year in the middle stratosphere, even though they are at similar latitudes and seasons (September). The data were taken during different years (1996 versus 1993), so some of the difference may be due to interannual dynamical variability effects which are not contained in the model. At high latitudes, the model agrees fairly well with the late winter observations in March taken outside of the polar vortex at 68°N (Figure 9f, squares), and the summer observations at 65°N (Figure 9e). However, the model did not capture the very old air (8-10 years) observed inside the vortex above 20 km at 68°N during March (Figure 9f, asterisks). We also note that a few measurements of Γ as old as 8-9 years at 20-25 km are shown in the June profile at 65°N. These data are significantly older than the model and reflect the fact that this OMS balloon flight passed through remnants of the winter/spring polar vortex (F. Moore and E. Ray, private communication, 1998). The model also shows a region of reduced vertical age gradients at 10-17 km in the summer profile at 65°N which is indicated in the data. This model feature at these levels is characteristic of middle and high latitudes during summer and fall in both hemispheres (Figure 7).

Figures 8 and 9 also show the mean age from our previous 1995 model version (dotted line) which was discussed in the ^{14}C and ^{90}Sr simulations (section 3.3). Relative to the observations and the 1999 model simulation, Γ from the 1995 model is significantly underestimated, and the associated latitudinal and vertical gradients are much flatter. This is consistent with the 1995 model simulation of ^{14}C and ^{90}Sr and reflects the overly strong diffusive and advective nature of this previous model transport.

While these model simulations assume that SF_6 is an inert tracer, it is possible that SF_6 incurs a small photochemical loss in the mesosphere. This loss rate is currently not well characterized. If such a loss exists, it would cause the observed Γ in Figures 8 and 9 to be overestimated. Including such a loss in the simulations would increase the model-inferred lag time to be older than the base simulation of Γ shown above. *Hall and Waugh* [1998] found that the inferred mean age in the high-latitude middle stratosphere can be significantly affected when imposing simple mesospheric loss rates on SF_6 simulated in 3-D models. To test the influence of a mesospheric SF_6 loss in our model, we included a loss identical to C_2ClF_5 (CFC-115) in our 1999 model simulation in Figures 8 and 9 (dashed line). The CFC-115 photolytic losses are taken from *DeMore et al.* [1997] and result in a lifetime of about 600 years in our model. Significant increases in the model-inferred age occur at middle and high latitudes and at the higher altitudes in the tropics when including this mesospheric loss. At 20 km (Figure 8), Γ is generally 0.5 to 1 year older at middle to high latitudes, with ages increased by nearly 2 years at the SH pole during spring. This latter result reflects the mesospheric character of air within the SH vortex, even at levels reaching down to the lower

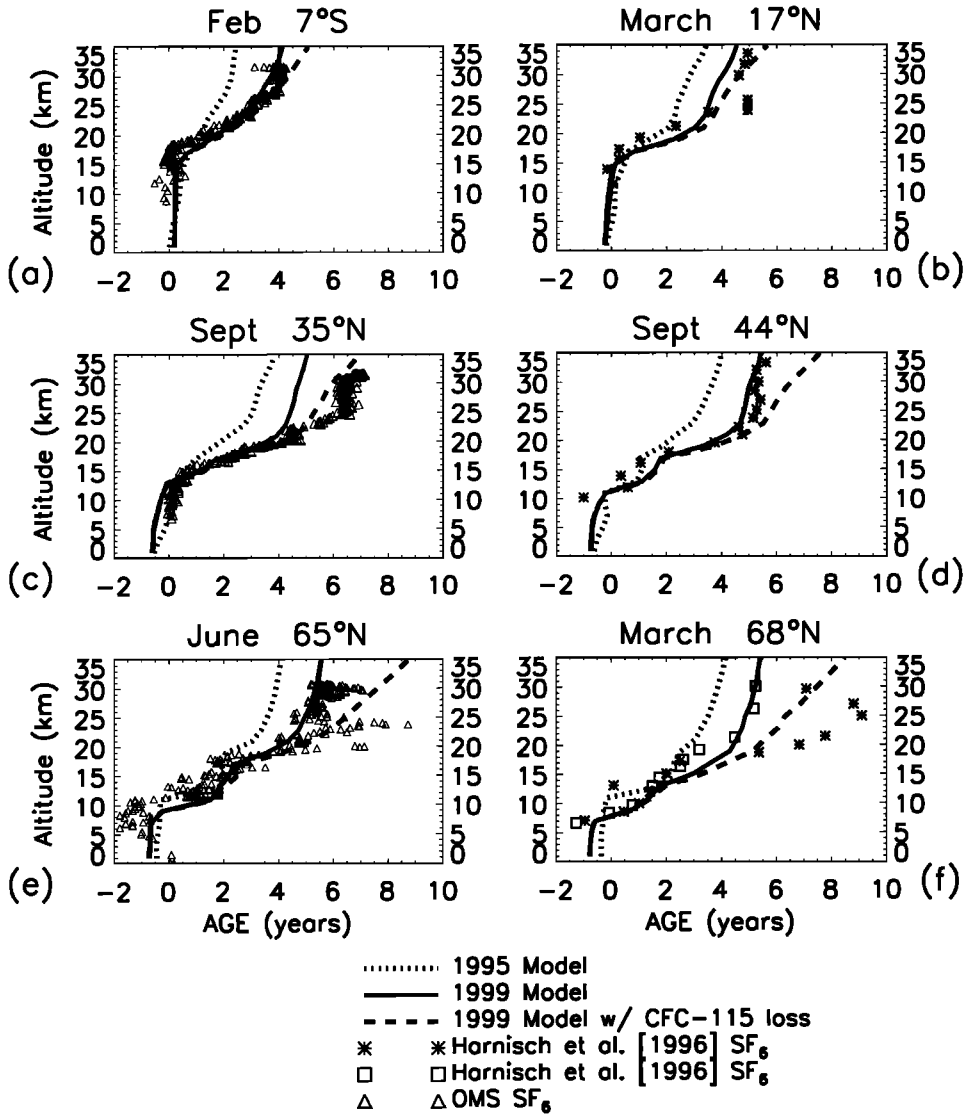

Figure 9. Vertical profiles of age of air derived from SF_6 from the model and balloon data taken at the latitudes and seasons indicated. The observations are from OMS data (triangles) and the balloon data of *Harnisch et al.* [1996] (asterisks and squares). Included are model simulations using the previous 1995 model transport (dotted line), the 1999 transport (solid line), and the 1999 transport with a photochemical loss identical to CFC-115 imposed on SF_6 (dashed line). The age is taken relative to the global mean value at the surface.

stratosphere. In Figure 9, including the mesospheric loss increased Γ in the mid-stratosphere by 1 year at low latitudes, 2 years at middle latitudes, and 3 years at high latitudes.

Overall, it is not clear if the model Γ is in better agreement with the data at the higher altitudes and/or latitudes when including this mesospheric loss. The comparisons inside the NH vortex are improved; however, the model still underestimates the observations by 1 to 2 years (Figure 9f, asterisks). The agreement is also improved at 35°N (Figure 9c), but is worsened at 44°N (Figure 9d) when including the mesospheric loss. Furthermore, the data generally show a sharp reduction in the vertical gradient near 25-30 km with little or no gradient above this level. The standard 1999 model shows this characteristic shape, whereas the model with the mesospheric loss indicates a continued increase in Γ with increasing altitude above 25 km.

We emphasize that we are not attempting to fully explain the model-measurement differences in Figures 8 and 9 by including a loss rate comparable to CFC-115 in the model simulations. Such a loss rate is considered a probable upper limit and is shown here primarily as a qualitative example of how such a loss could affect the model Γ. Furthermore, analysis of Γ derived from OMS SF_6 and CO_2 data, with the latter corrected for CH_4 oxidation, shows that the SF_6 ages are older than the CO_2 ages by only 1 year or less (J.W. Elkins et al., manuscript in preparation, 1999). Since CO_2 does not undergo any net photochemical loss in the stratosphere,

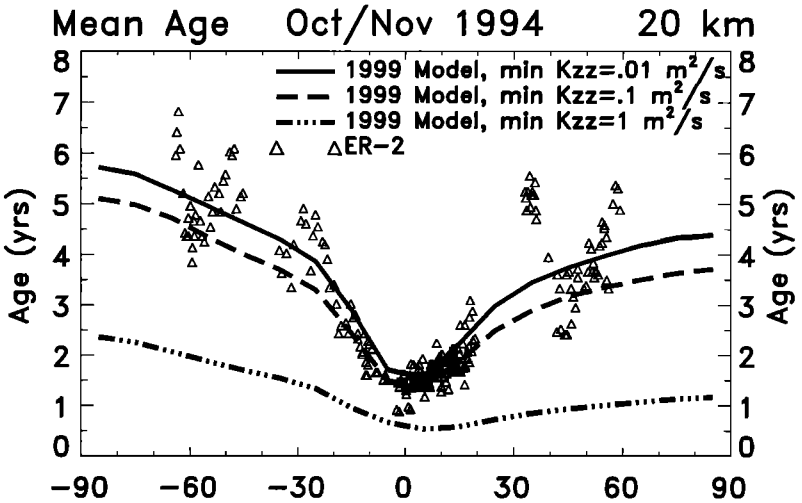

Figure 10. Age of air derived from SF_6 as a function of latitude for October/November 1994. The ER-2 observations (triangles) are identical to Figure 8. The model simulations are for 20 km and include the standard 1999 model as in Figure 8 (solid line), the standard 1999 model with the minimum lower stratospheric K_{zz} increased to 0.1 m^2s^{-1} (dashed line), and the standard 1999 model with the minimum lower stratospheric K_{zz} increased to 1 m^2s^{-1} (dash-triple dot line). No mesospheric loss is imposed on SF_6.

this suggests that a photochemical loss of SF_6, if one exists, is smaller than the CFC-115 loss. Certainly, better laboratory characterization of the mesospheric loss incurred by SF_6 is needed.

Differences between the base model simulation and observations in Figures 8 and 9 probably also reflect limitations of the model formulation. Figures 8 and 9 show that the model-measurement agreement is fairly good in the very lower stratosphere below ~20 km. However, in some of the comparisons, the model shows a tendency to increasingly underestimate the observed Γ with increasing height above 22-25 km, especially in the NH vortex region. This discrepancy does not appear to be caused by the model having too strong of a circulation in the upper stratosphere and mesosphere. Model sensitivity tests reveal that significantly decreasing the mesospheric gravity wave drag and hence the global circulation throughout the upper stratosphere and mesosphere increases the simulated Γ by only 2 months at 35 km. Discrepancies within the NH polar vortex seen in Figure 9f are probably due to the fact that the vortex is frequently centered off the pole and exhibits large year to year variability and, as such, cannot be resolved by the current zonal mean climatological model formulation. In contrast, the model does a reasonable job in qualitatively resolving the SH vortex (Figures 1 and 7), which has smaller longitudinal and interannual variability.

3.5. Age of Air Sensitivity to K_{zz}

An important transport component in 2-D models is the vertical eddy diffusivity (K_{zz}). In the mesosphere, diffusion coefficients can be determined from gravity wave parameterizations [e.g., *Lindzen*, 1981], which provide for reasonably good long-lived tracer simulations [e.g., *Garcia and Solomon*, 1985; *Chandra et al.*, 1997]. Determination of K_{zz} in the upper troposphere and lower stratosphere is very important for proper treatment of the tropopause boundary and troposphere-stratosphere exchange processes. In this region of our model, K_{zz} is proportional to the vertical temperature gradient which gives a large K_{zz} in the troposphere and very small mixing in the lower stratosphere. We specify a minimum K_{zz} of 0.01-0.02 m^2s^{-1} in the lower stratosphere following observational analyses [*Hall and Waugh*, 1997b; *Mote et al.*, 1998].

An evaluation of the lower stratospheric vertical diffusion specified in models was recently made by *Hall et al.* [1999]. These authors discussed the influence of K_{zz} on the propagation of seasonal signals in the tropics and concluded that a value of $K_{zz} < 0.1$ m^2s^{-1} is most realistic. Here we illustrate the sensitivity of the model global distribution of Γ to the lower stratospheric minimum in K_{zz}. This will help to evaluate the qualitative realism of our new model K_{zz} field.

Figures 10 and 11 show the mean age from the base 1999 model simulation along with the SF_6 observations as shown in Figures 8 and 9. We also include two additional model scenarios in which the lower stratospheric minimum K_{zz} is increased to 0.1 m^2s^{-1} and 1 m^2s^{-1}, respectively, but are otherwise identical to the base 1999 model. Increasing the minimum rate of vertical mixing reduces the mean age throughout the stratosphere. Increasing the minimum to 0.1 m^2s^{-1} decreases Γ only slightly in the tropical lower stratosphere, but the difference increases to as much as 0.75 years in the middle stratosphere and in the lower stratosphere extratropics.

With a minimum K_{zz} of 1 m^2s^{-1}, Γ is signicantly

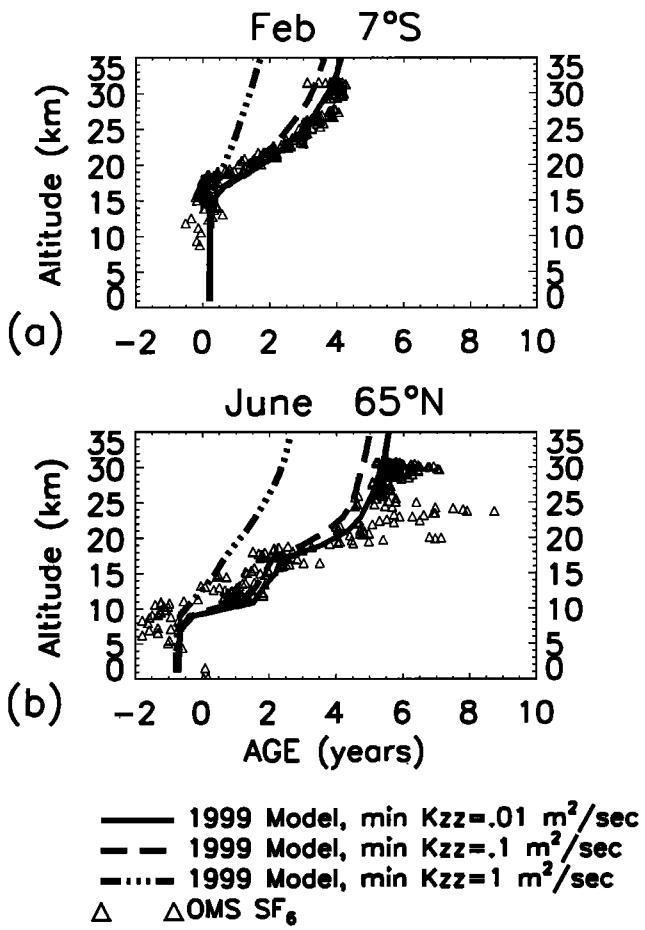

Figure 11. Vertical profiles of age of air from the model and OMS balloon SF_6 data taken at the latitudes and seasons indicated. The OMS observations are as in Figure 9. The model simulations include the standard 1999 model as in Figure 9 (solid line), the standard 1999 model with the minimum lower stratospheric K_{zz} increased to 0.1 m^2s^{-1} (dashed line), and the standard 1999 model with the minimum lower stratospheric K_{zz} increased to 1 m^2s^{-1} (dash-triple dot line). No mesospheric loss is imposed on SF_6.

younger everywhere compared to observations and the base model scenario. Maximum differences of ~3 years occur at middle and high latitudes in the middle stratosphere. In addition, both the vertical and horizontal gradients in mean age are drastically reduced in this model run. This unrealistic scenario is far outside the range of the observations and is similar to the "diffusive regime" discussed by *Hall et al.* [1999] in their analysis of seasonal signal propagation. Although the model scenario with the minimum K_{zz} set to 0.1 m^2s^{-1} is within the observational values of Γ, the overall model-measurement agreement is not as good relative to the base model case. This provides evidence that a minimum K_{zz} of 0.01-0.02 m^2s^{-1} is most realistic, as was suggested by the analyses of *Hall and Waugh* [1997b] and *Mote et al.* [1998]. Our model-measurement comparisons of CH_4 also reveal that a minimum K_{zz} of 0.01-0.02 m^2s^{-1} gives the most realistic model simulation.

It is interesting to note the sensitivity to K_{zz} of the meridional gradients in Figure 10. Previous attempts to modify modeled gradients between the tropics and midlatitudes have focussed on changes to K_{yy} [e.g., *Weisenstein et al.*, 1996]. However, Figure 10 reveals that vertical transport is also important in determining the isolation of the tropics from midlatitudes.

3.6. Seasonal Cycle in Carbon Dioxide

The source of carbon dioxide at the ground includes a secular trend of ~1.4 ppmv/yr along with a large biosphere-induced seasonal cycle. This seasonal variation is largest at high northern latitudes and is strongly latitude dependent. At stratospheric levels, CO_2 is nearly inert: it has no photochemical loss and has only a small production from CH_4 oxidation. The transport characteristics of the stratosphere are therefore reflected in the propagation of the CO_2 seasonal cycle. As shown in previous observational analyses, the stratospheric signal originates at the tropical tropopause and propagates vertically in the tropics with a gradual loss of amplitude. Just above the tropopause, the CO_2 signal is also transported rapidly poleward with only a small decrease in amplitude. At higher altitudes (above ~460 K, ~19 km) the midlatitude signal is very small, indicating that the barrier to poleward transport from the tropics becomes increasingly strong with height [*Strahan et al.*, 1998; *Mote et al.*, 1998]. Simulation of these characteristics in CO_2 therefore provides a diagnostic of model transport.

Our time dependent model simulation of CO_2 uses lower boundary conditions based on monthly mean global surface observations for 1979 to 1995 [*Conway et al.*, 1994]. The simulation was continued through 1997 by increasing the 1995 boundary conditions by 1.4 ppmv/yr. To properly compare with observations, the model is run with all photochemistry included so that the small CO_2 source from CH_4 oxidation is accounted for. This simulation also includes the corresponding time dependent surface boundary conditions of CH_4 [*WMO*, 1995]. Figure 12 shows the model simulated annual cycle amplitude of CO_2, defined as one-half of the difference from peak to trough of the seasonal variation. The amplitude maximizes at the ground in the northern hemisphere extratropics (~7.5 ppmv) and decreases equatorward and with increasing height in the troposphere. There is a sharp decrease in amplitude (and phase lag, not shown) across the tropopause into the lower stratosphere, especially in the NH extratropics. This illustrates a strong separation between the model troposphere and stratosphere and is consistent with observations showing that the CO_2 seasonal cycle in the NH midlatitude lower stratosphere is propagated from the tropics and not from the underlying troposphere [e.g., *Strahan et al.*, 1998].

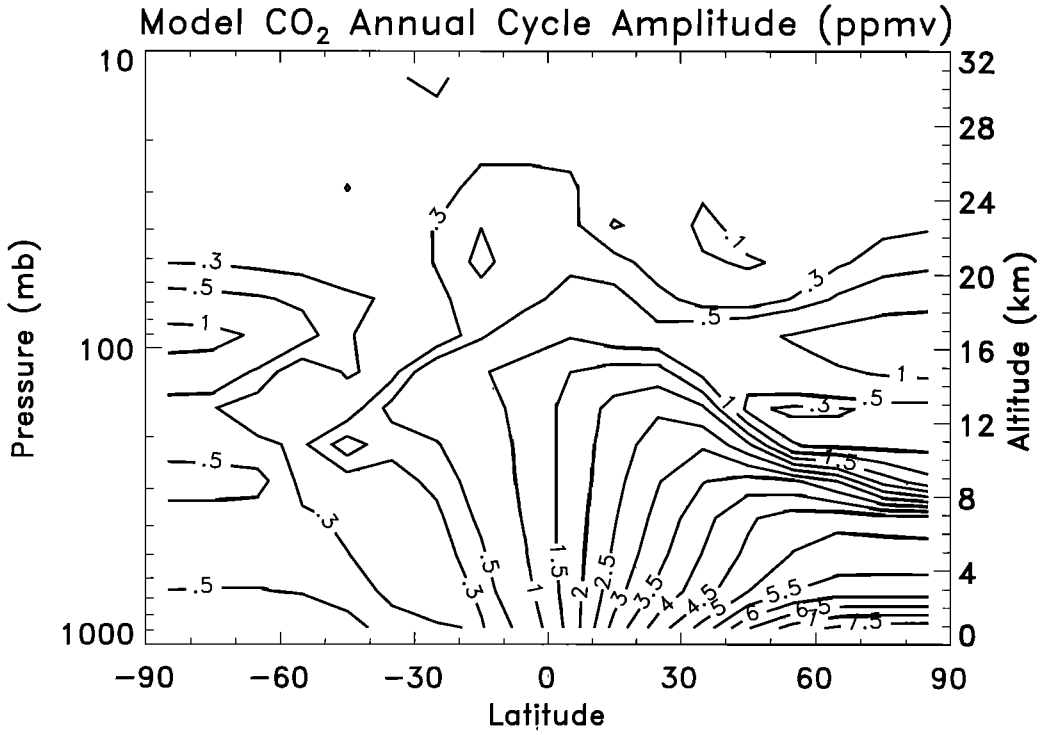

Figure 12. Latitude-height cross section of the model amplitude of the annual cycle of CO_2 (ppmv), defined as one-half of the difference from peak to trough of the seasonal variation. The contour interval is 0.5 ppmv and includes the 0.1 and 0.3 ppmv contours.

The model simulation in certain regions of the stratosphere can be compared with CO_2 observations from the ER-2 field campaigns [*Boering et al.*, 1996]. We first examine the simulation at the tropical tropopause, which essentially is the boundary condition for CO_2 entering the the stratosphere. Figure 13 shows CO_2 time series for 1992 through 1997 of model simulations using the 1999 transport (solid line) and the previous 1995 transport (dotted line), along with the ER-2 observations. Here we have plotted the ER-2 data just

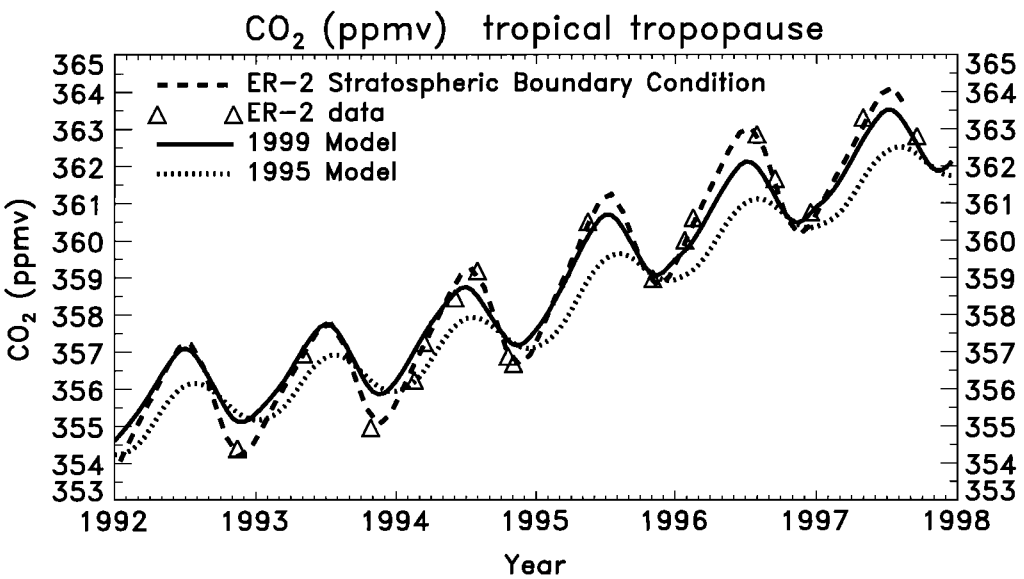

Figure 13. Time series of CO_2 (ppmv) at the tropical tropopause for 1992 through 1997. Included are model simulations using the previous 1995 model transport (dotted line) and the 1999 transport (solid line), along with averages of ER-2 CO_2 measurements taken just above the tropopause from *Boering et al.* [1996] (triangles), and the stratospheric boundary condition time series based the ER-2 CO_2 measurements (dashed line). See text for details.

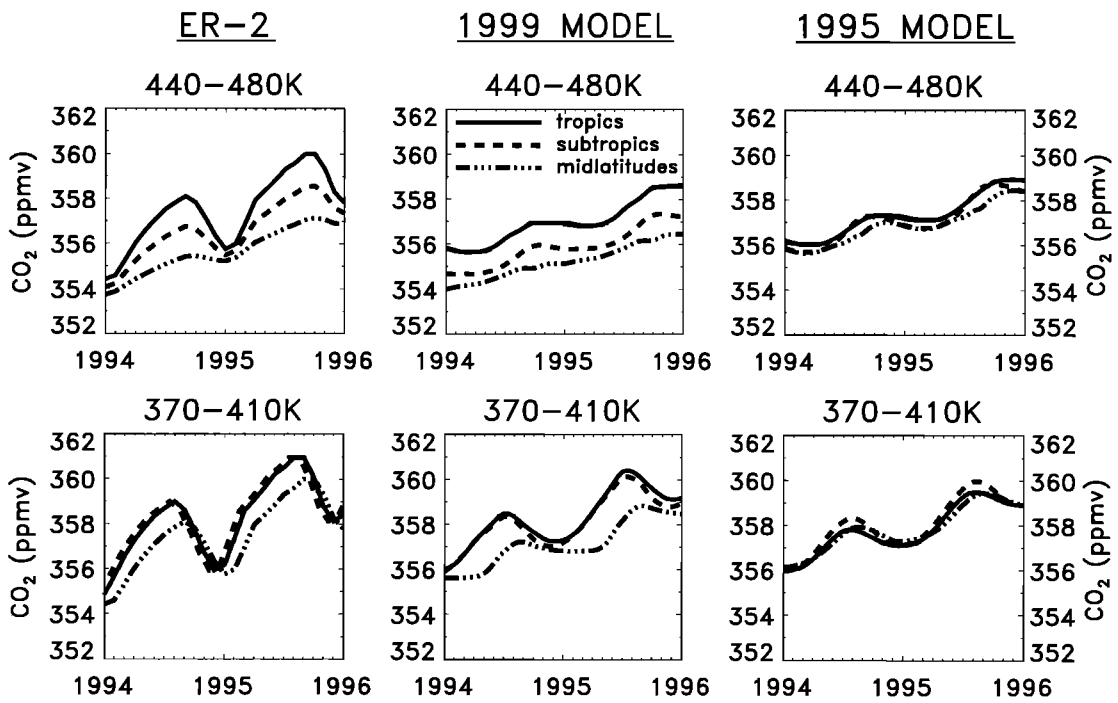

Figure 14. Time series of CO_2 (ppmv) for 1994 and 1995 based on ER-2 observations and model simulations at 370-410 K and 440-480 K for three latitude ranges: tropics (6°S-12°N, solid line), subtropics (12°N-30°N, dashed line), and midlatitudes (30°N-48°N, dashed-triple dot line). The observations are least squares fits to the seasonal cycle and trend and are adapted from *Strahan et al.* [1998]. Included are model simulations using the 1999 transport (middle column) and the previous 1995 model transport (right-hand column). The data and model have been binned by N_2O. See text for details.

above the tropical tropopause [*Boering et al.*, 1996; *Andrews et al.*, 1999] (triangles), along with the stratospheric boundary condition time series of the ER-2 CO_2 measurements (dashed line) discussed in *Andrews et al.* [1999].

The phase of the 1999 model simulation in Figure 13 agrees quite well with the observations. However, the 1999 model amplitude is underestimated by roughly a third (1.1 versus 1.6 ppmv). At least part of this amplitude deficiency is due to the coarse vertical resolution (~2 km) of the model which cannot fully resolve the very sharp transition in mixing observed around the tropopause region. This issue will be addressed in future versions of the model with improved resolution. It also appears that the 1999 model does not fully resolve the observed changes in the secular trend in CO_2. This is reflected by the fact that in the early part of the period, the model captures the observed maxima fairly well but underestimates the minima, with this tendency reversed in the latter part of the period. This discrepancy probably reflects deficiencies in the model tropospheric transport, although inconsistencies between the observed CO_2 surface boundary condition used in the model and the ER-2 stratospheric measurements may also contribute to the difference. As was shown in the previous comparisons, the 1999 model in Figure 13 is in significantly better agreement with the data compared to the 1995 model transport. The 1995 model amplitude is 40% smaller (0.65 ppmv versus 1.1 ppmv), and the phase is lagged by about 2 months relative to the 1999 model.

To check the propagation of the CO_2 seasonal cycle throughout the lower stratosphere, Figure 14 compares the 1999 and 1995 model simulations at several latitudes and levels with time series representing the ER-2 data for 1994 and 1995 adapted from *Strahan et al.* [1998]. The ER-2 curves are least squares fits to a combination of the estimated stratospheric input seasonal cycle and the observed linear trend at stratospheric midlatitudes. The data are binned by N_2O for three latitude ranges: tropics (6°S-12°N), subtropics (12°N-30°N), and midlatitudes (30°N-48°N), and for two potential temperature (Θ) ranges: 370-410 K (very near the tropopause) and 440-480 K (18-20 km). The model values represent the averages for the same latitude and Θ ranges used for the observations.

Near the tropopause (370-410 K), the observations show very similar seasonal amplitudes and phases in the tropics and subtropics, illustrating the strong coupling of these regions. At midlatitudes, some amplitude attenuation and phase delay relative to the lower latitudes is observed, indicating a weak isolation of the

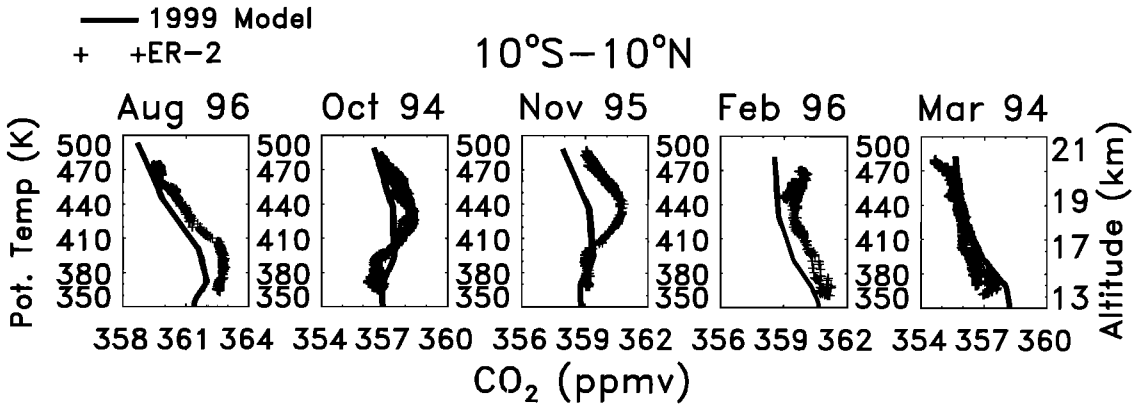

Figure 15. Vertical profiles of CO_2 (ppmv) versus potential temperature (K) from the model (solid line) and ER-2 measurements (crosses) for 10°S to 10°N for the month/year indicated. Approximate altitude is shown on the right-hand axes.

midlatitudes from the subtropics. The 1999 model qualitatively captures these features, including the strong coupling of the tropics and subtropics. Somewhat more amplitude attenuation at midlatitudes is simulated than observed, suggesting that the model slightly underestimates the poleward transport out of the subtropics. The phase lag and decreased amplitude at midlatitudes illustrate that the 1999 model seasonal cycle at 370-410 K is being transported poleward from the tropical lower stratosphere and not from the underlying troposphere. The 1995 model amplitudes in the tropics and subtropics are somewhat weaker than simulated by the 1999 model, consistent with the difference in amplitudes at the tropical tropopause seen in Figure 13. However, a more notable discrepancy in the 1995 model at 370-410 K is the lack of separation between the middle and lower latitudes seen in the observations and the 1999 model. This suggests that the 1995 model has overly strong tropical-midlatitude transport at these levels and/or the model extratropical lower stratosphere undergoes excessive mixing with the underlying troposphere.

At the upper level (440-480 K), both the 1999 model and data show a steady amplitude decrease and very little phase change with increasing latitude. At midlatitudes, both show very little seasonal cycle with mainly the secular increase in CO_2 evident. This indicates that poleward mixing of tropical air is significantly weaker than at lower levels, and/or extratropical mixing processes damp out the seasonal cycle at midlatitudes. However, the 1999 model results show a systematic underestimation of the observed amplitudes which is particularly acute in the tropics and subtropics. This is due in part to the underestimation, by roughly a third, of the signal amplitude entering at the tropical tropopause (Figure 13), which then biases the model simulation throughout the stratosphere. There also may be inadequacies in the model which further overattenuate the signal in the stratosphere. Nevertheless, the 1999 model simulation shows qualitative consistency with the observations and illustrates that the 1999 model reproduces the tropical-midlatitude transport in a reasonable manner. In contrast to both the data and the 1999 model, the 1995 model at 440-480 K shows very little amplitude change between the three latitude regions, suggesting a lack of tropical isolation and excessively strong mixing between the tropics and midlatitudes at this level.

To supplement these model-data comparisons, we show vertical profiles of the ER-2 and the 1999 model CO_2 plotted against potential temperature (Θ) in the tropical lower stratosphere in Figure 15. Here the plots are arranged by season (independent of year) to illustrate the propagation of the seasonal cycle with altitude. A maximum is observed just above the tropical tropopause (380-400 K) during August, reflecting the entry into the stratosphere of the seasonal maximum during June/July (see Figure 13). This maximum progresses to higher levels during the following months. Likewise, a minimum is seen at 380-400 K during October-November, progressing up to 430-440 K during February and at or above 480 K in March. The model shows some indication of this signal propagation; however, the amplitude is underestimated, as was seen in Figure 14. Again, this is probably due to an underestimation of the signal entering the stratosphere and to an overattenuation of the signal amplitude in the model stratosphere.

Figure 16 compares vertical profiles of the ER-2 and 1999 and 1995 model CO_2 for 30°N-40°N and 70°S-60°S for the months indicated. Here we use N_2O as the vertical coordinate given that, unlike the tropics, CO_2 and Θ are not highly correlated in the extratropics. The tropospheric source of N_2O is seasonally invariant and undergoes only a small secular increase which is contained in our model simulations. In the lower stratosphere, CO_2 and N_2O form a compact relationship, since both have very long chemical timescales and will be similarly affected by the seasonal variations in transport. There-

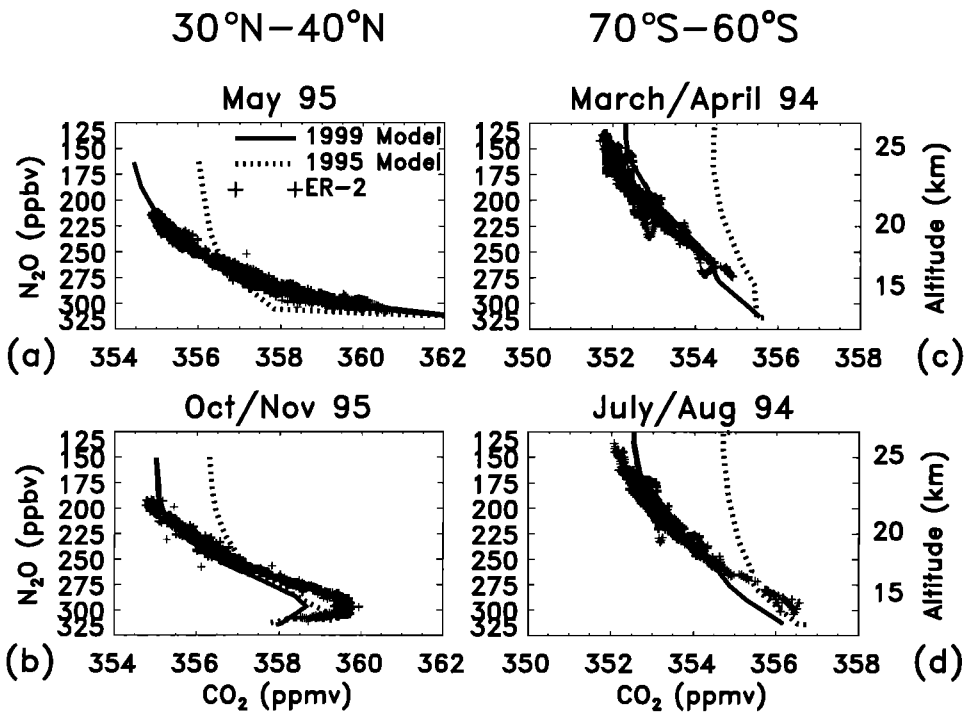

Figure 16. Vertical profiles of CO_2 (ppmv) versus N_2O (ppbv) for 30°N to 40°N (left-hand column) and 70°S to 60°S (right-hand column) for the month/year indicated. Included are the ER-2 measurements (crosses) and model simulations using the previous 1995 model transport (dotted line) and the 1999 transport (solid line). Approximate altitude is shown on the right-hand axes.

fore variations in CO_2 for a given value of N_2O will be due only to the transport of the seasonal cycle and trend of the CO_2 source.

The 1999 model $CO_2 - N_2O$ relationship in Figure 16 shows good overall consistency with the data. At 30°N-40°N during October/November 1995, the observed CO_2 maximum at $N_2O = 300$ ppbv is qualitatively simulated by the 1999 model. This reflects the separation between tropospheric air at the lowest altitudes and stratospheric air above, as was seen in Figure 12. The model maximum is not as sharp as seen in the data, which may reflect the coarse model grid resolution as was discussed in Figure 13. At 70°S-60°S, the 1999 model shows a slightly weaker vertical CO_2 gradient than observed, and this discrepancy occurs similarly throughout the year (other seasons not shown). At these latitudes the seasonal amplitude at all levels is small (see Figure 12) so that CO_2 exhibits primarily a secular increase. This model-data difference may reflect, in part, incomplete resolution of the CO_2 trend entering the model stratosphere as was seen in Figure 13. This difference may also indicate inadequacies in the model N_2O photochemistry.

The 1995 model $CO_2 - N_2O$ correlations in Figure 16 are significantly different from both the observations and the 1999 model. The 1995 model significantly overestimates the observed CO_2 at $N_2O < 250$ ppbv at 30°N-40°N and at almost all levels at 70°S-60°S. This is consistent with the global-wide underestimation of the mean age seen in Figures 8 and 9 and the model-data differences in ^{14}C and ^{90}Sr (Figures 5 and 6). This results from an overly strong diffusive and advective transport on a global basis in the 1995 model. These transport inaccuracies also cause deficiences in the simulation of the CO_2 seasonal cycle which are reflected in the 1995 model-data differences at the lower levels ($N_2O > 275$ ppbv) at 30°N-40°N in Figures 16a and 16b.

As seen in Figure 14, the seasonal amplitude in both the model and data decreases substantially with increasing height and latitude away from the tropical tropopause, with only very small amplitudes at the NH midlatitudes above ~ 18 km. Therefore it is interesting that the model indicates secondary amplitude maxima centered near 16 km poleward of 60° in both hemispheres in Figure 12. These features appear to be due to descent within the polar vortices during winter and early spring. Low CO_2 values are advected downward, resulting in late winter/early spring minima and hence significant seasonal cycle amplitudes. This effect maximizes at the poles and is evident at 15-20 km, where there is a substantial vertical gradient in CO_2. Above 20 km, there is little vertical CO_2 gradient, so that the downward motion has little effect on the seasonal cycle. This feature was not indicated in previous model simulations of the CO_2 seasonal cycle [*Hall and Prather*,

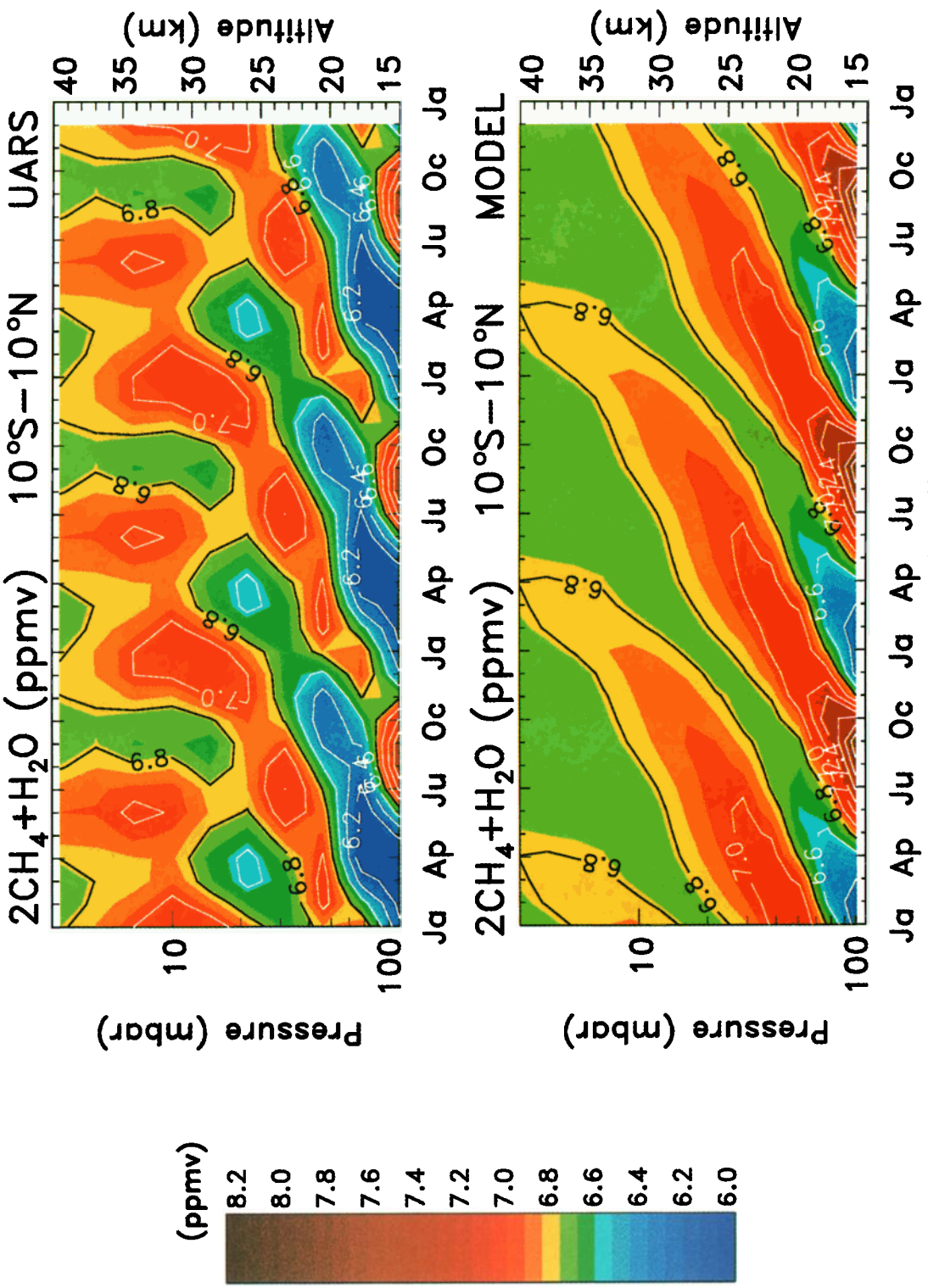

Plate 1. Zonal mean annual time series, repeated for 3 years, of $2CH_4 + H_2O$ (ppmv) averaged from 10°S to 10°N from the UARS climatology (top) and the 1999 model simulation (bottom). The values are shown in color and in the overlaid contours in intervals of 0.2 ppmv.

1993; *Waugh et al.*, 1997; *Strahan et al.*, 1998]. It would be difficult to validate this feature with the ER-2 data, given the limited temporal coverage of these observations. Since this feature does not seem to be related to the seasonal cycle in the CO_2 source, extracting information from the data by fitting a tropospheric annual cycle and trend as was done by *Strahan et al.* [1998] would not seem to be justified in this case.

3.7. Tropical Transport of $2CH_4 + H_2O$ ($\hat{H}$)

To supplement the seasonal cycle propagation of CO_2, we now discuss the modeled and observed seasonal variation of the quasi-conserved quantity, $2CH_4 + H_2O$ (defined as $\hat{H}$ following *Mote et al.* [1998]) in the equatorial lower stratosphere. Plate 1 shows the model simulation along with the UARS combined climatology [*Randel et al.*, 1998], both repeated for 3 years. The annual cycle in the lower and middle stratosphere is qualitatively captured in the model. This seasonal variation is driven by the annual cycle in H_2O at the tropical tropopause. Dry (moist) air enters the stratosphere during the NH winter (summer), coincident with the coldest (warmest) tropopause temperatures. This seasonal variation is advected slowly upward by the residual circulation and maintains its structure for a long time period because of the weak horizontal and vertical diffusion characteristic of the tropical lower stratosphere [e.g., *Mote et al.*, 1996]. While the UARS data show evidence of a semiannual cycle in the middle stratosphere above 30 km, the model simulates an SAO signal only in the upper stratosphere above 40 km (see Figure 1b).

The amplitude and phase lag based on Fourier analysis of the annual harmonic of the $\hat{H}$ seasonal signal are shown in Figure 17. Here the quantities plotted are relative to those at the tropical tropopause. The model phase lag variation with height shows good agreement with the data, although the model propagates the signal a bit faster between 50 and 10 mbar. Between 100 and 10 mbar, the average phase propagation of the model is about 0.37 mm/s compared to 0.34 mm/s in the observations. However, a more notable discrepancy is that the model amplitude attenuates faster with increasing altitude compared to observations. This difference was characteristic of the various models analyzed in the MMII intercomparisons [*Hall et al.*, 1999]. Part of this discrepancy is due to the fact that HALOE underestimates the H_2O annual cycle near the tropopause [e.g., *Mote et al.*, 1996; *Andrews et al.*, 1999], resulting in an overestimation of the fractional amplitude at higher altitudes. However, as shown in Figures 14 and 15, the model CO_2 simulation in the lower tropical stratosphere suggests a larger seasonal amplitude decrease with height compared to the ER-2 in situ data. Moreover, inspection of Plate 1 reveals that while there is reasonable model-HALOE agreement in simulating regions of large $\hat{H}$ (> 6.8 ppmv), regions where $\hat{H}$ < 6.6 ppmv are not as well resolved in the model. Therefore some of the $\hat{H}$ amplitude discrepancy in Figure 17a is probably due to difficiencies in the model.

To investigate the processes that affect the seasonal signal propagation in this region, we have plotted our model transport fields in the lower-middle tropical strato-

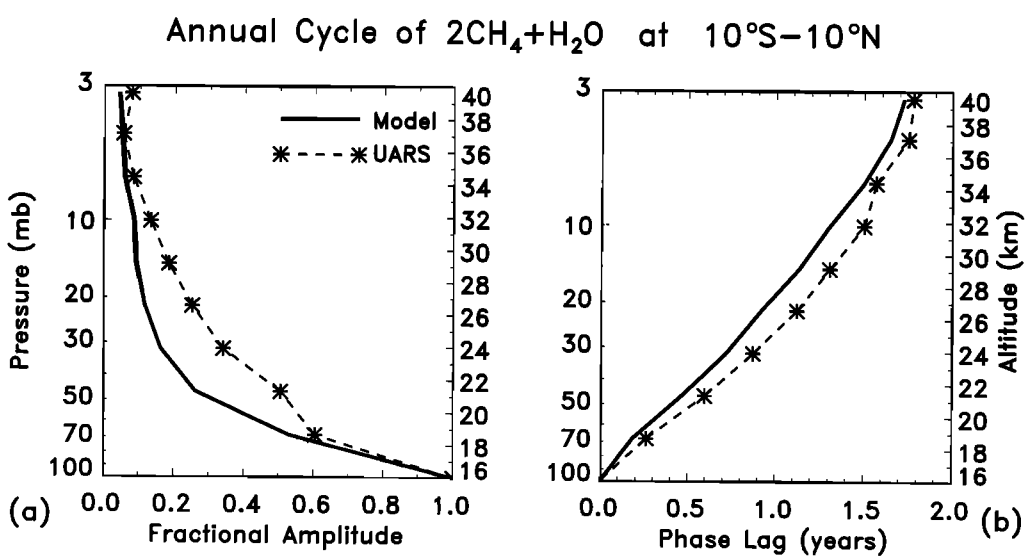

Figure 17. Vertical profiles of the (a) fractional amplitude and (b) phase lag of the annual cycle in $2CH_4 + H_2O$ at 10°S to 10°N from the 1999 model (solid line) and the UARS climatology (dashed-asterisk line). These quantities were obtained by Fourier analysis of the values shown in Plate 1. The amplitude has been normalized to the value at the tropical tropopause (100 mbar), and the phase lag (years) is defined to be zero at the tropical tropopause.

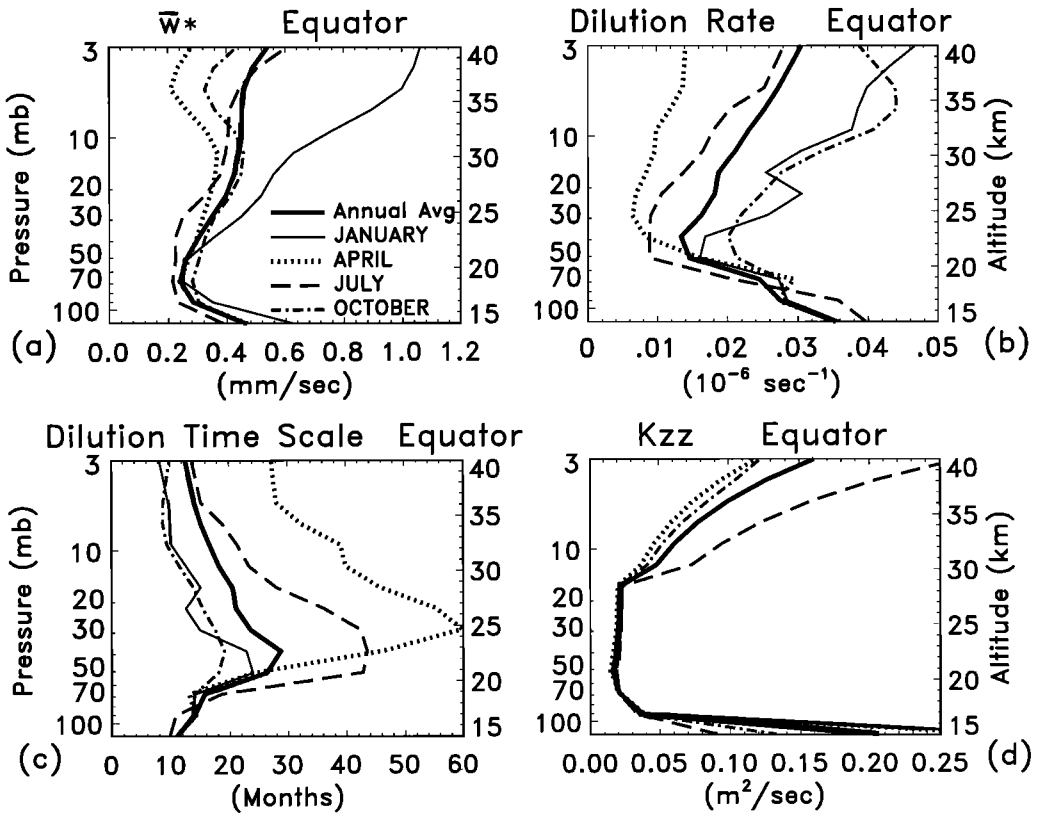

Figure 18. Vertical profiles of the 1999 model dynamics in the lower stratosphere at the equator for January (thin solid), April (dotted), July (dashed), October (dash-dot), and the annual mean (heavy solid). The dilution rate (10^{-6}s^{-1}) and its reciprocal, the dilution timescale (months), are estimates of the horizontal in-mixing of midlatitude air and are based on the model K_{yy} values (see text for details). Also included are the residual vertical velocity (mm/s) and the vertical diffusion, K_{zz}(m^{2}s^{-1}).

sphere in Figure 18. These can be compared with those derived from HALOE data by *Mote et al.* [1998]. Here we present values for the different seasons along with the annual average. The annual mean residual vertical velocity ($\bar{w}^*$) is in good agreement with the Mote et al. analysis, with a minimum of 0.22 mm/s at 19-21 km, increasing with height to about 0.4 mm/s at 30 km. The average phase propagation of 0.37 mm/s in the model $\hat{H}$ in Figure 17b generally reflects the average vertical velocity between 16 and 32 km. The minimum $\bar{w}^*$ at 19-25 km contributes to a slowing of the phase propagation at these altitudes in Figure 17b, although this feature is weaker than observed. Consistent with previous findings, the seasonal variations in the lower stratosphere reveal a maximum $\bar{w}^*$ during NH winter (January) and a minimum during the SH winter (July). There is also especially strong upwelling above 30 km during January. This seasonal variability is attributed to the greater extratropical planetary wave driving during the NH winter compared to the SH winter. This, in turn, controls the seasonal variations of the vertical mass flux in the lower tropical stratosphere [e.g., *Rosenlof*, 1995; *Mote et al.*, 1996]. The seasonal variation in $\bar{w}^*$ is thought to be responsible for the seasonal temperature cycle at the tropical tropopause, which in turn, drives the seasonal signal in water vapor reflected in Plate 1. The model vertical diffusion rates in Figure 18d are specified to be generally consistent with observational analyses [*Hall and Waugh*, 1997b; *Mote et al.*, 1998] (see section 2). Values are 0.01-0.02 m^{2}s^{-1} at 17-29 km and increase to greater than 0.1 m^{2}s^{-1} above 30 km.

To provide a rough estimate of the dilution rate of midlatitude air into the tropics, we computed the area-weighted average K_{yy} value for 35°S-35°N divided by the equator to 35° distance squared, which is taken as the characteristic length scale of mixing into the tropics from the midlatitudes of each hemisphere. The results in Figure 18 reveal a minimum annual mean dilution rate (maximum time scale) near 22 km. This is qualitatively consistent with observational analyses that suggest that the tropics are considerably more isolated from the midlatitudes above about 19 km than below [e.g., *Schoeberl et al.*, 1997; *Mote et al.*, 1998]. This was also seen in the CO_2 comparisons in Figure 14. Our maximum annual mean timescale near 22 km is about 2.5

years, a bit longer than reported by other previous studies [e.g., *Schoeberl et al.*, 1997; *Hall and Waugh*, 1997b; *Randel et al.*, 1998] but much shorter than the 6-7 year timescale derived by *Mote et al.* [1998].

The model dilution parameters plotted in Figures 18b and 18c are meant to provide a rough estimate of the mixing of midlatitude air into the tropics. There are substantial spatial and seasonal variations in the model K_{yy} field across the 35°S-35°N region which affect the computed dilution rate. In Figures 18b and 18c, the seasonal variability of the entrainment of midlatitude air into the tropics is driven largely by the seasonal variations in extratropical planetary wave activity. For example, tropical dilution during January and July occurs preferentially from the winter hemisphere, owing to the large planetary wave mixing occurring in the winter subtropics and midlatitudes. Similarly, the strong dilution during October occurs preferentially from the SH, due to the large wave activity occurring in the SH subtropics and midlatitudes during spring. The weak wave activity in both hemispheres during April is reflected in the relatively small tropical dilution rates during this season seen in Figures 18b and 18c.

As discussed by *Mote et al.* [1998] and *Hall et al.* [1999], entrainment of midlatitude air is largely responsible for the attenuation of the observed tape recorder signal in the lower tropical stratosphere, although vertical diffusion is also important despite the relatively small values. The observed entrainment is a minimum at 19-25 km, which coincides with the reduced attenuation of the tape recorder signal in Figure 17a. Although the model overattenuates the seasonal amplitude relative to the observations in this region, it is not clear that this is due to overentrainment of midlatitude air in the model. The model dilution timescales above 20 km are quantitatively consistent with some observational studies, although they are significantly shorter than reported in the *Mote et al.* [1998] analysis. To test if the model entrainment rates are too large, we set K_{yy} to a very small value of $1\text{x}10^8\text{cm}^2\text{s}^{-1}$ throughout the year at 35°S to 35°N in the lower and middle stratosphere. This corresponds to a dilution timescale of 48 years and produces a very isolated tropical region. However, the corresponding attenuation of the $\hat{H}$ seasonal amplitude was only somewhat diminished and was still significantly greater than observed between 20 and 27 km. This suggests that the entrainment of midlatitude air in our standard model is reasonable and is not the major cause of the model seasonal signal overattenuation.

Increasing the model vertical diffusion may effectively reduce the signal attenuation to be closer to observations. However, this will diminish the model-measurement agreement in other areas [*Hall et al.*, 1999]. For example, the phase of the signal will be propagated too quickly, and the vertical gradient of the age of air will be decreased (see section 3.5, Figure 11). Our model vertical velocity and vertical diffusion rates shown in Figure 18 are in fairly good agreement with the observations so that model discrepancies in these quantities do not seem to significantly contribute to the overattenuation. Numerical diffusion introduced by the advection scheme could artificially damp out the signal; however, such diffusion is generally small in the current scheme [*Lin and Rood*, 1996]. It is possible that the overattenuation is caused by the relatively coarse vertical resolution of the model (~2 km), which may not enable the simulation to properly resolve the propagation of the observed seasonal signals. This possibility will be addressed in future work.

4. Conclusions

We have developed a new empirically based transport formulation for use in our GSFC 2-D transport and chemistry model. To derive the transport fields, the formulation utilizes empirically based zonal mean zonal wind, temperature, diabatic and latent heating rates, E-P flux diagnostics for planetary- and synoptic-scale waves, and parameterizations to account for the effects due to gravity waves and equatorial Kelvin waves. As such, this scheme utilizes significantly more information compared to our previous methodology, which was based only on zonal mean temperatures and heating rates.

To evaluate this new transport, we performed several diagnostic tests and presented extensive model-measurement comparisons of several long-lived tracers in the upper troposphere and stratosphere. The model captures much of the qualitative spatial and seasonal variability seen in satellite and aircraft observations. These include the isolation of the tropics and the well-mixed surf-zone region of the winter midlatitudes. The model-data agreement in the low-latitude tracer gradients supports the use of the HRDI wind data to derive the model planetary wave driving and diffusion quantities in this region. At high latitudes the model captures the general isolation of the southern polar vortex. However, because of the large longitudinal and interannual variability at high northern latitudes in winter, much of the NH vortex structure gets smoothed out when zonally averaging meteorological data sets. Therefore the model cannot adequately resolve the observed isolation of the NH vortex.

The model total ozone field captures much of the observed seasonal and latitudinal variability seen in the TOMS data. A major discrepancy occurs in the middle to high southern latitudes in which the model does not resolve the spring breakup of the Antarctic ozone hole and, subsequently, maintains larger than observed latitudinal gradients during the southern high-latitude summer. Sensitivity tests reveal that this deficiency is not due to an underestimation of horizontal mixing during the breakup of the southern polar vortex and points to other processes that are not accurately resolved in the model.

Simulations of carbon 14 and strontium 90 reproduced the observed peak in mixing ratio at 20-25 km and the decrease with altitude in mixing ratio above 25 km. The latitudinal and vertical gradients of the simulated mean age of air derived from SF_6 compare well with aircraft and balloon observations in the lower stratosphere below 20-22 km and outside of the NH polar winter vortex. To qualitatively illustrate how a mesospheric loss rate for SF_6 would introduce an error in the calculation of Γ, we included a loss identical to that of CFC-115 (corresponding to a ~600 year atmospheric lifetime) in the SF_6 simulation. This increased the age of air by as much as 3 years in the high-latitude middle stratosphere. However, it was inconclusive as to whether including this loss rate provided better overall model agreement with the balloon data above 25 km. It is likely that if SF_6 does incur a mesospheric loss, it is somewhat smaller than the CFC-115 loss rate. Certainly better laboratory characterization of the SF_6 loss is needed.

The propagation of the seasonal signal in carbon dioxide from the tropical lower stratosphere to midlatitudes is qualitatively reproduced by the model, and the model simulates the observed near absence of seasonal variability at higher levels at midlatitudes. However, simulations of both CO_2 and $\hat{H}$ show that the model attenuates the seasonal signals too rapidly with altitude in the tropics, a characteristic that is consistent among many stratospheric models. We found that the model generally reproduces the altitudinal variation of horizontal entrainment of midlatitude air into the tropics as reported in several observational studies [e.g., *Schoeberl et al.*, 1997; *Mote et al.*, 1998]. Furthermore, the vertical phase propagation of $\hat{H}$ and the vertical gradient of the mean age are both consistent with the observations. These results, along with various sensitivity tests, suggest that the overattenuation of the seasonal signal cannot be fully explained by an overestimation of the horizontal in-mixing, the model explicit vertical diffusion, and/or numerical diffusion introduced by the numerical advection scheme. It is possible that this model deficiency is caused in large part by the coarse vertical and horizontal model resolution (~2 km by 10° latitude). The model with such resolution cannot sufficiently resolve and propagate the seasonal cycles, so that the amplitudes are effectively reduced.

We found that the circulation in the upper troposphere and stratosphere is determined by a combination of the empirically determined net heating rates, wave drive, and the bottom boundary condition in the lower troposphere. Changes in this circulation will affect methane, total ozone, mean age, and other diagnostic tracers in a consistent manner. For example, an overly strong circulation will overestimate (underestimate) CH_4 at low (high) latitudes, with the opposite tendency in total ozone, and produce a mean age that is too young at all latitudes. Obtaining reasonable model-measurement agreement in these tracers simultaneously at different latitudes and seasons gives confidence that the circulation is fairly consistent with the real atmosphere. Furthermore, the simulations with the new transport formulation are in substantially better agreement with observations compared to our previous model transport. Taken together, these model-measurement tracer comparisons therefore provide a rigorous test of the new model dynamics and demonstrate that such an empirically based zonal mean transport scheme can successfully reproduce many of the characteristic dynamical features observed in the stratosphere. This enables us to provide better model simulations of ozone for a variety of scientific and assessment studies.

Acknowledgments. The authors would like to thank Paul Newman for helpful discussions; S.J. Lin for helpful discussions concerning the numerical advection scheme and for making available his 1-D and 3-D numerical advection FORTRAN codes; Mark Burrage for supplying the HRDI level 2 wind data; Jochen Harnisch for the balloon SF_6 data; Susan Strahan for the seasonal cycle fits of the CO_2 data, and for helpful discussions concerning the data; Kristie Boering for the tropical tropopause CO_2 data; Bill Randel for the UARS climatologies of CH_4 and H_2O; and Jim Elkins, Fred Moore, and Eric Ray for making available the OMS SF_6 data and for helpful discussions concerning the data. We also thank the NASA Atmospheric Chemistry Modeling and Analysis Program and the UARS Science Investigation Program for support of this project.

References

Andrews, A.E., K.A. Boering, B.C. Daube, S.C. Wofsy, E.J. Hintsa, E.M. Weinstock, and T.P. Bui, Empirical age spectra for the lower tropical stratosphere from in situ observations of CO_2: Implications for stratospheric transport, *J. Geophys. Res.*, in press, 1999.

Andrews, D.G., J.R. Holton, and C.B. Leovy, *Middle Atmosphere Dynamics*, 498 pp., Academic, San Diego, Calif., 1987.

Bacmeister, J.T, M.R. Schoeberl, M.E. Summers, J. Rosenfield, and X. Zhu, Descent of long lived trace gases in the winter polar vortex, *J. Geophys. Res., 100*, 11669-11684, 1995.

Barnett, J.J., and K. Labitzke, Climatological distribution of planetary waves in the middle atmosphere, *COSPAR International Reference Atmosphere: 1986, Part II: Middle Atmosphere Models, Adv. Space Res., 10*, (12), 63-91, 1990.

Boering, K.A., S.C. Wofsy, B.C. Daube, H.R. Schneider, M. Loewenstein, J.R. Podolske, and T.J. Conway, Stratospheric mean ages and transport rates from observations of carbon dioxide and nitrous oxide, *Science, 274*, 1340-1343, 1996.

Carpenter, R.L., Jr., K.K. Droegemeier, P.R. Woodward, and C.E. Hane, Application of the piecewise parabolic method (PPM) to meteorological modeling, *Mon. Weather Rev., 118*, 586-612, 1990.

Chandra, S., C.H. Jackman, A.R. Douglass, E.L. Fleming, and D.B. Considine, Chlorine catalyzed destruction of ozone: Implications for ozone variability in the upper stratosphere, *Geophys. Res. Lett., 20*, 351-354, 1993.

Chandra, S., C.H. Jackman, E.L. Fleming, and J.M. Russell III, The seasonal and long term changes in mesospheric water vapor, *Geophys. Res. Lett., 24*, 639-642, 1997.

Choi, W.K., and J.R. Holton, Transport of N_2O in the

stratosphere related to the equatorial semiannual oscillation, *J. Geophys. Res., 96*, 22543-22557, 1991.

Colella, P., and P.R. Woodward, The piecewise parabolic method (PPM) for gas-dynamical simulations, *J. Comput. Phys., 54*, 174-201, 1984.

Conway, T.J., P.P. Tans, L.S. Waterman, K.W. Thoning, D.R. Kitzis, K.A. Masarie, and N. Zhang, Evidence for interannual variability of the carbon cycle from the NOAA Climate Monitoring and Diagnostics Laboratory Global Air Sampling Network, *J. Geophys. Res., 99*, 22831-22855, 1994.

DeMore, W.B., S.P. Sander, D.M. Golden, R.F. Hampson, M.J. Kurylo, C.J. Howard, A.R. Ravishankara, C.E. Kolb, and M.J. Molina, Chemical kinetics and photochemical data for use in stratospheric modeling, Evaluation number 12, *JPL Publ., 97-4*, 266 pp., 1997.

Douglass, A.R., C.H. Jackman, and R.S. Stolarski, Comparison of model results transporting the odd nitrogen family with results transporting separate odd nitrogen species, *J. Geophys. Res., 94*, 9862-9872, 1989.

Douglass, A.R., C.J. Weaver, R.B. Rood, and L. Coy, A three-dimensional simulation of the ozone annual cycle using winds from a data assimilation system, *J. Geophys. Res., 101*, 1463-1474, 1996.

Dunkerton, T.J., On the role of the Kelvin wave in the westerly phase of the semi-annual zonal wind oscillation, *J. Atmos. Sci., 36*, 32-41, 1979.

Elkins, J.W., et al., Airborne gas chromatograph for in situ measurements of long-lived species in the upper troposphere and lower stratosphere, *Geophys. Res. Lett., 23*, 347-350, 1996.

Fleming, E.L., S. Chandra, J.J. Barnett, and M. Corney, Zonal mean temperature, pressure, zonal wind, and geopotential height as functions of latitude, *COSPAR International Reference Atmosphere: 1986, Part II: Middle Atmosphere Models, Adv. Space Res., 10*, (12), 11-59, 1990.

Garcia, R.R., and S. Solomon, A numerical model of the zonally averaged dynamical and chemical structure of the middle atmosphere, *J. Geophys. Res., 88*, 1379-1400, 1983.

Garcia, R.R., and S. Solomon, The effect of breaking gravity waves on the dynamics and chemical composition of the mesosphere and lower thermosphere, *J. Geophys. Res., 90*, 3850-3868, 1985.

Garcia, R.R., F. Stordal, S. Solomon, and J.T. Kiehl, A new numerical model of the middle atmosphere, 1. Dynamics and transport of tropospheric source gases, *J. Geophys. Res., 97*, 12967-12991, 1992.

Geller, L.S., J.W. Elkins, J.M. Lobert, A.D. Clarke, D.F. Hurst, J.H. Butler, and R.C. Myers, Tropospheric SF_6: Observed latitudinal distribution and trends, derived emissions and interhemispheric exchange time, *Geophys. Res. Lett., 24*, 675-678, 1997.

Gray, L.J., and J.A. Pyle, Two-dimensional model studies of equatorial dynamics and tracer distributions, *Q.J.R. Meteorol. Soc., 113*, 635-651, 1987.

Hall, T.M., and M.J. Prather, Simulations of the trend and annual cycle in stratospheric CO_2, *J. Geophys. Res., 98*, 10573-10581, 1993.

Hall, T.M., and R.A. Plumb, Age as a diagnostic of stratospheric transport, *J. Geophys. Res., 99*, 1059-1070, 1994.

Hall, T.M., and D.W. Waugh, Timescales for the stratospheric circulation derived from tracers, *J. Geophys. Res., 102*, 8991-9001, 1997a.

Hall, T.M., and D.W. Waugh, Tracer transport in the tropical stratospheric due to vertical diffusion and horizontal mixing, *Geophys. Res. Lett., 24*, 1383-1386, 1997b.

Hall, T.M., and D.W. Waugh, Influence of nonlocal chemistry on tracer distributions: Inferring the mean age of air from SF_6, *J. Geophys. Res., 103*, 13327-13336, 1998.

Hall, T.M., D.W. Waugh, K.A. Boering, and R.A. Plumb, Evaluation of transport in stratospheric models, *J. Geophys. Res.*, in press, 1999.

Harnisch, J., R. Borchers, P. Fabian, and M. Maiss, Tropospheric trends for CF_4 and C_2F_6 since 1982 derived from SF_6 dated stratospheric air, *Geophys. Res. Lett., 23*, 1099-1102, 1996.

Haynes, P.H., C.J. Marks, M.E. McIntyre, T.G. Shepherd, and K.P. Shine, On the "downward control" of extratropical diabatic circulations by eddy-induced mean zonal forces, *J. Atmos. Sci., 48*, 651-678, 1991.

Holton, J.R., and X. Zhu, A further study of gravity wave induced drag and diffusion in the mesosphere, *J. Atmos. Sci., 41*, 2653-2662, 1984.

Huang, T.Y.W., and A.K. Smith, The mesospheric diabatic circulation and the parameterized thermal effect of gravity wave breaking on the circulation, *J. Atmos. Sci., 48*, 1093-1111, 1991.

Jackman, C.H., A.R. Douglass, R.B. Rood, R.D. McPeters, and P.E. Meade, Effect of solar proton events on the middle atmosphere during the past two solar cycles as computed using a two-dimesional model, *J. Geophys. Res., 95*, 7417-7428, 1990.

Jackman, C.H., A.R. Douglass, K.F. Brueske, and S.A. Klein, The influence of dynamics on two-dimensional model results: Simulations of ^{14}C and stratospheric NO_x injections, *J. Geophys. Res., 96*, 22559-22572, 1991.

Jackman, C.H., E.L. Fleming, S. Chandra, D.B. Considine, and J.E. Rosenfield, Past, present, and future modeled ozone trends with comparisons to observed trends, *J. Geophys. Res., 101*, 28753-28767, 1996.

Kinnison, D. E., H. S. Johnston, and D.J. Wuebbles, Model study of atmospheric transport using carbon 14 and strontium 90 data as inert tracers, *J. Geophys. Res., 99*, 20647-20664, 1994.

Lin, S.-J., and R.B. Rood, Multidimensional flux-form semi-Lagrangian transport schemes, *Mon. Weather Rev., 124*, 2046-2070, 1996.

Lindzen, R. S., Turbulence and stress owing to gravity wave and tidal breakdown, *J. Geophys. Res., 86*, 9707-9714, 1981.

Lipson, J.B., M.J. Elrod, T.W. Beiderhase, L.T. Molina, and M.J. Molina, Temperature dependence of the rate constant and branching ratio for the OH + ClO reaction, *J. Chem. Soc. Faraday Trans., 93*, 2665-2673, 1997.

Mote, P.W., K.H. Rosenlof, M.E. McIntyre, E.S. Carr, J.C. Gille, J.R. Holton, J.S. Kinnersley, H.C. Pumphrey, J.M. Russell III, and J.W. Waters, An atmospheric tape recorder: The imprint of tropical tropopause temperatures on stratospheric water vapor, *J. Geophys. Res., 101*, 3989-4006, 1996.

Mote, P.W., T.J. Dunkerton, M.E. McIntyre, E.A. Ray, P.H. Haynes, and J.M. Russell III, Vertical velocity, vertical diffusion, and dilution by midlatitude air in the tropical lower stratosphere, *J. Geophys. Res., 103*, 8651-8666, 1998.

Newell, R.E., J.W. Kidson, D.G. Vincent, and G.J. Boer, *The General Circulations of the Tropical Atmosphere*, vol. 2, chap. 7, MIT Press, Cambridge, Mass., 1974.

Park, J. H., M. K. W. Ko, C. H. Jackman, R. A. Plumb, and K. H. Sage (eds.), Models and Measurements II, NASA Langley Res. Cent., Hampton, Va., in press, 1999.

Patra, P.K., S. Lal, B.H. Subbaraya, C.H. Jackman, and P. Rajaratnam, Observed vertical profile of sulphur hexafluoride (SF_6) and its atmospheric applications, *J. Geophys. Res., 102*, 8855-8859, 1997.

Prather, M.J., Numerical advection by conservation of second-order moments, *J. Geophys. Res., 91*, 6671-6681, 1986.

Prather, M.J., and E.E. Remsberg, The atmospheric effects of stratospheric aircraft: Report of the 1992 Models and Measurements Workshop, *NASA Ref. Publ., 1292*, vols. 1-3, 1993.

Randel, W.J., and R.R. Garcia, Application of a planetary wave breaking parameterization to stratospheric circulation statistics, *J. Atmos. Sci., 51*, 1157-1168, 1994.

Randel, W.J., B.A. Boville, J.C. Gille, P.L. Bailey, S.T. Massie, J.B. Kumer, J.L. Mergenthaler, and A.E. Roche, Simulation of stratospheric N_2O in the NCAR CCM2: Comparison with CLAES data and global budget analyses, *J. Atmos. Sci., 51*, 2834-2845, 1994.

Randel, W.J., F. Wu, J.M. Russell III, A. Roche, and J.W. Waters, Seasonal cycles and QBO variations in stratospheric CH_4 and H_2O observed in UARS HALOE data, *J. Atmos. Sci., 55*, 163-185, 1998.

Ray, E.A., F.L. Moore, J.W. Elkins, G.S. Dutton, D.W. Fahey, H. Vomel, S.J. Oltmans, and K.H. Rosenlof, Transport into the Northern Hemisphere lowermost stratosphere revealed by in situ tracer measurements, *J. Geophys. Res.*, in press, 1999.

Rinsland, C.P., M.R. Gunson, M.C. Abrams, L.L. Lowes, R. Zander, and E. Mahieu, ATMOS/ATLAS 1 measurements of sulfur hexafluoride SF_6 in the lower stratosphere and upper troposphere, *J. Geophys. Res., 98*, 20491-20494, 1993.

Rosenfield, J.E., P.A. Newman, and M.R. Schoeberl, Computations of diabatic descent in the stratospheric polar vortex, *J. Geophys. Res., 99*, 16677-16689, 1994.

Rosenfield, J.E., D.B. Considine, P.E. Meade, J.T. Bacmeister, C.H. Jackman, and M.R. Schoeberl, Stratospheric effects of Mount Pinatubo aerosol studied with a coupled two-dimensional model, *J. Geophys. Res., 102*, 3649-3670, 1997.

Rosenlof, K.H., Seasonal cycle of the residual mean meridional circirculation in the stratosphere, *J. Geophys. Res., 100*, 5173-5191, 1995.

Schoeberl, M.R., D.F. Strobel, and J.P. Apruzese, A numerical model of gravity wave breaking and stress in the mesosphere, *J. Geophys. Res., 88*, 5249-5259, 1983.

Schoeberl, M.R., A.E. Roche, J.M. Russell III, D. Ortland, P.B. Hays, and J.W. Waters, An estimation of the dynamical isolation of the tropical lower stratosphere using UARS wind and trace gas observations of the quasi-biennial oscillation, *Geophys. Res. Lett., 24*, 53-56, 1997.

Solomon, S., R.W. Portmann, R.R. Garcia, L.W. Thomason, L.R. Poole, and M.P. McCormick, The role of aerosol variations in anthropogenic ozone depletion at northern midlatitudes, *J. Geophys. Res., 101*, 6713-6727, 1996.

Stolarski, R.S., et al., Scientific assessment of the atmospheric effects of stratospheric aircraft, *NASA Ref. Publ., 1381*, 110 pp., 1995.

Strahan, S.E., A.R. Douglass, J.E. Nielsen, and K.A. Boering, The CO_2 seasonal cycle as a tracer of transport, *J. Geophys. Res., 103*, 13729-13741, 1998.

Volk, C.M., J.W. Elkins, D.W. Fahey, G.S Dutton, J.M. Gilligan, M. Loewenstein, J.R. Podolske, K.R. Chan, and M.R. Gunson, Evaluation of source gas lifetimes from stratospheric observations, *J. Geophys. Res., 102*, 25543-25564, 1997.

Waugh, D.W., et al., Three-dimensional simulations of long-lived tracers using winds from MACCM2, *J. Geophys. Res., 102*, 21493-21513, 1997.

Weisenstein, D.W., M.K.W. Ko, N.D. Sze, and J.M. Rodriguez, Potential impact of SO_2 emissions from stratospheric aircraft on ozone, *Geophys. Res. Lett., 23*, 161-164, 1996.

World Meteorological Organization (WMO), Scientific Assessment of Ozone Depletion: 1994, *Rep. 37*, Global Ozone Res. and Monitoring Proj., Geneva, 1995.

D. B. Considine, E. L. Fleming, C. H. Jackman, and R. S. Stolarski, NASA Goddard Space Flight Center, Code 916, Greenbelt Road, Greenbelt, MD 20771-0001. (fleming@kahuna.gsfc.nasa.gov)

(Received January 26, 1999; revised May 6, 1999; accepted May 11, 1999.)